J. Webster (ed.), *Wiley Encyclopedia of Electrical and Electronics Engineering*

RADAR SIGNAL DETECTION

Each day, we constantly make decisions. Given certain hypotheses, information is selected on which to base each decision, and under certain conditions, we may need to determine the reliability of the information. Such is the case in radar signal detection: A returned signal is received, and we have to decide whether a target is present or absent. If there were no noise or interference, the decision could be made with complete confidence. However, in reality, the received signal is usually heavily corrupted by environmental noise, interference, and noise from the radar system itself, and so on. In order to make a reliable decision, the noise and unwanted signals have to be suppressed with a so-called matched filter before a decision can be made.

Owing to the existence of noise and interference, radar signal detection has to be treated as a statistical problem, regardless of whether the signal under detection is deterministic or not. This statistical formalism of radar signal detection theory can be applied to all types of radar signals without restriction. To understand radar signal detection, noise has to be quantitatively described. A time-limited deterministic signal can be described as a time series, and a periodic deterministic signal can be represented as a Fourier series. In contrast, noise cannot be represented as a deterministic function in the time or frequency domains. In other words, we cannot predict a noise-contaminated radar signal with absolute certainty. However, with available noise information such as the expectation, the power, or even the probability distribution of noise, we can select a criterion on which to base our decision.

Concepts of Signal-to-Noise Ratio and Matched Filter

The signal-to-noise ratio (*SNR*) in radar and communication systems is defined as

$$\text{SNR} = \frac{(\text{signal power})}{(\text{noise variance})} \qquad (1)$$

The maximum output SNR, the most frequently used criterion for radar detection, is defined as the ratio of the maximum instantaneous output signal power to the output noise power. The input SNR is a major limiting factor for radar detection performance.

For a fixed input SNR, a linear time-invariant filter whose frequency response function maximizes the output SNR is called a *matched filter*. Matched filtering transforms the raw radar data into a form that is suitable for (1) generating the optimal decision for detection; (2) estimating the target parameters with a minimal rms error, or (3) obtaining the maximum resolving power for a group of targets. The characteristics of matched filters can be described by either a frequency-domain transfer function or a time-domain impulse response function, each being related to the other by the Fourier transform. In the frequency domain, the matched-filter transfer function $H(\omega)$ is the complex conjugate of the spectrum of the signal. Thus, in general terms

$$H(\omega) = kS^*(\omega)e^{-j\omega T} \qquad (2)$$

where $S(\omega)$ is the spectrum of the input signal $s(t)$ and T is a delay constant required to make the filter physically realizable. The normalizing factor k and the delay constant are generally ignored in formulating the underlying significant relationship. This simplification yields

$$H(\omega) = S^*(\omega) \tag{3}$$

Equation (3) reveals that the bandwidth of the receiver must be the same as that of the signal. This is understandable, because if the bandwidth of the receiver is wide compared with that occupied by the signal energy, extraneous noise may be introduced into the excess bandwidth, which lowers the output signal-to-noise ratio. On the other hand, if the receiver bandwidth is narrower than the signal bandwidth, the noise energy is reduced along with part of the signal energy. The result is again a lowered SNR. When the receiver bandwidth is identical to the signal bandwidth as in the case of the matched filter, the output SNR is maximized. The conjugate in Eqs. (2) and (3) allows the phases of $S(\omega)$ and $H(\omega)$ to cancel each other out, and leaves the output signal spectrum a linear phase, $e^{-j\omega T}$, which results in a peak at the time instant T in the output.

The corresponding time-domain relationship between the signal to be detected and the matched filter is obtained from the inverse Fourier transform of $H(\omega)$. This leads to the result that the impulse response of a matched filter is a replica of the time inverse of the known signal function. Thus, if $h(t)$ represents the matched-filter impulse response, the relationship equivalent to Eq. (2) is given by

$$h(t) - ks(T - t) \tag{4}$$

As before, k and T can be ignored to yield the basic relationship

$$h(t) = s(-t) \tag{5}$$

Figure 1 illustrates the relationship given by Eqs. (3) and (5), where $s(t)$ is a pulsed linear frequency-modulated (*LFM*) signal with the form

$$s(t) = \begin{cases} \sin[2\pi(t - 1.2)^2], & t \in [1.2, 1.6] \\ 0, & \text{otherwise} \end{cases} \tag{6}$$

The phase from $H(\omega)$ is the negative of that from $S(\omega)$, while $h(t)$ is the time reversal of the $s(t)$.

Figure 2(a) shows a received signal, which is the signal $s(t)$ of Eq. (6) corrupted by a 6 dB Gaussian noise; that is, the input SNR is -6 dB. It is difficult to detect the existence of the signal $s(t)$ from this figure. However, after the received signal is processed by the matched filter, the detector output peak in Fig. 2(b) clearly indicates the existence of the signal.

The output from the matched filter, as shown in Fig. 3, is the convolution between the received signal and the matched-filter impulse response, that is,

$$\begin{aligned} y(t) &= \int_0^t [s(\tau) + n(\tau)]h(t - \tau)\, d\tau \\ &= \int_0^t [s(\tau) + n(\tau)]s(T - t + \tau)\, d\tau \end{aligned} \tag{7}$$

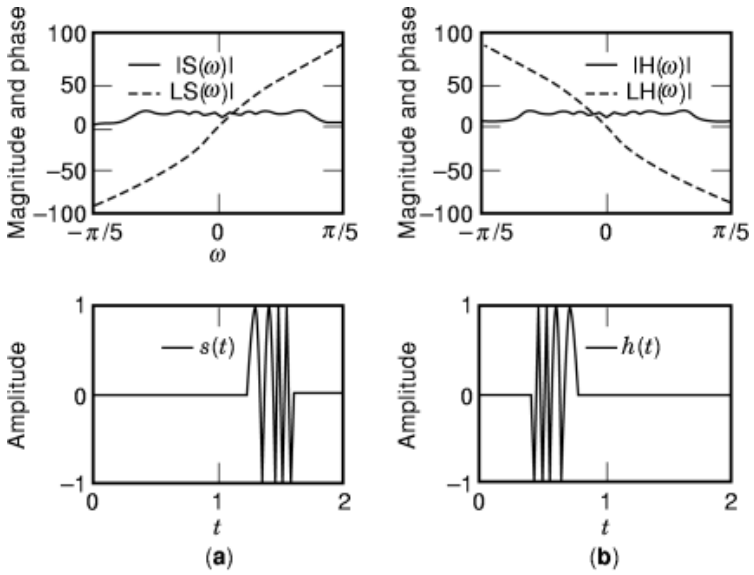

Fig. 1. (a) Signal $s(t)$ and (b) matched-filter $h(t)$ relations. Phase in units of degrees. The phase from $H(\omega)$ is the negative of that from $S(\omega)$, while $h(t)$ is the time reversal of $s(t)$.

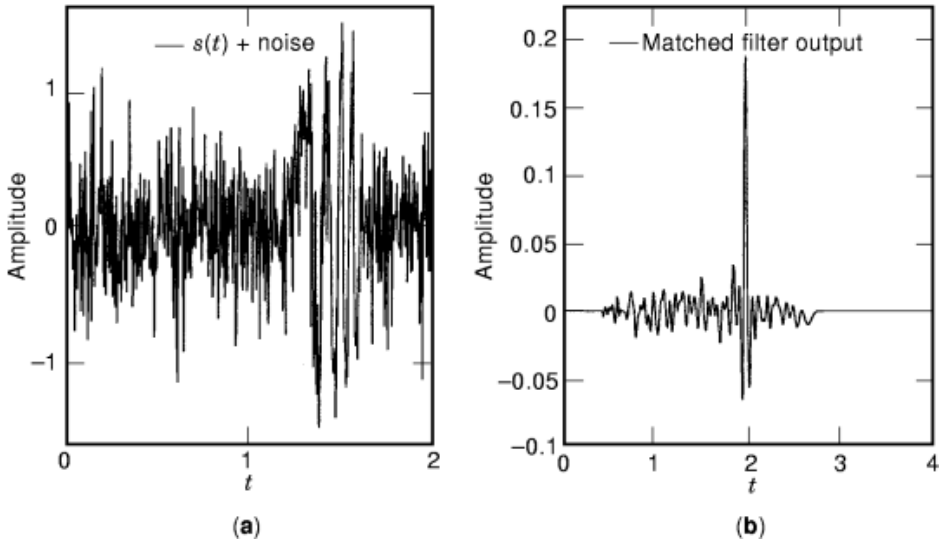

Fig. 2. (a) Signal corrupted by noise and (b) the matched-filter output. The peak in the matched-filter output indicates the existence of the signal.

Sampling $y(t)$ at $t = T$ yields the maximum output signal value, that is,

$$\begin{aligned} y(t)_{\max} = y(T) &= \int_0^T [s(\tau) + n(\tau)]s(\tau)\,d\tau \\ &= E_s + \int_0^T n(\tau)s(\tau)\,d\tau \end{aligned} \tag{8}$$

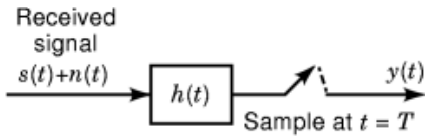

Fig. 3. Block diagram of a matched filter.

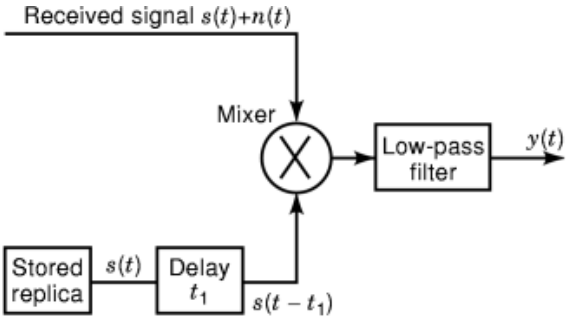

Fig. 4. Block diagram of a cross-correlation, which is another implementation of the matched filter.

where E_s represents the signal energy. It can be easily verified that the expectation of $y(t)_{max}$ is E_s, because the second term in Eq. (8) represents the noise whose mean is zero. This can be easily seen from Fig. 2(b) in which the maximum signal energy occurs at $t = T = 2$, and the maximum value is close to the expectation of $E_s = 0.18$ in this experiment. A detailed analysis of the matched filter will be given in the section entitled "Analysis of a Matched Filter."

Equation (7) describes the output of the matched filter as the cross-correlation between the received signal and a replica of the transmitted signal. This implies that the matched filter can be replaced by a cross-correlation that performs the same mathematical operation, as shown in Fig. 4. The received signal is multiplied by a delayed replica of the transmitted signal $s(t - t_1)$, and the product is passed through a low-pass filter. The cross-correlation tests for the presence of a target at only one time: t_1. Targets at other time delays, or ranges, may be found by varying t_1. However, this requires a longer search time. The search time can be reduced by adding parallel channels, each containing a delay line corresponding to a particular value of t_1, as well as a multiplier and a low-pass filter.

Since the cross-correlation and the matched filter are equivalent mathematically, the choice of which one to use in a particular radar application is determined by the practicality of implementation. The matched filter, or an approximation, has been generally preferred in the vast majority of applications.

Decision Criteria for Radar Signal Detection

The statistical detection problem consists of examining the received radar waveform $r(t)$ in a resolution cell to determine which of the following two hypotheses is true. The first hypothesis H_1 asserts that a target is present, and the received signal contains the target signature and noise. The second hypothesis H_0 states that the target is absent, and only noise is present in the received signal. The problem can be compactly stated as

$$\begin{aligned} H_1: &\quad r(t) = s(t) + n(t) \\ H_0: &\quad r(t) = n(t) \end{aligned} \tag{9}$$

The conditional probability density function completely describes the received signal statistically in both cases:

$$\begin{aligned} p(r|H_1) &= \text{conditional probability density function with} \\ &\quad \text{target present} \\ p(r|H_0) &= \text{conditional probability density function with} \\ &\quad \text{target absent} \end{aligned} \tag{10}$$

For reasons of simplicity, r is assumed to be a single sampled point of the received radar signal. The extension from a single sampled point to multiple sampled points is straightforward. The likelihood ratio is defined as

$$\Lambda(r) = \frac{p(r|H_1)}{p(r|H_0)} \tag{11}$$

The likelihood ratio $\Lambda(r)$ is also called the likelihood statistic. It is a random variable since it is a function of the random variable r. The *maximum likelihood* (*ML*) *decision criterion*, which chooses the hypothesis that most likely causes the observed signal, is

$$\Lambda(r) \underset{H_0}{\overset{H_1}{\gtrless}} 1 \tag{12}$$

This expression means that H_1 is selected if $\Lambda(r)$ is greater than 1; otherwise H_0 is selected. It can be seen that the ML criterion is a very simple decision criterion.

To describe the detection performance better, the probabilities of detection and false alarm are used in radar detection. The probability of detection refers to the probability of asserting the presence of a target when the target is indeed present

$$P_{\mathrm{d}} = \int_{R_0}^{\infty} p(r|H_1)\, dr \tag{13}$$

where R_0 is the decision boundary. The proper value of the boundary R_0 depends upon the criterion of decision. The probability of false alarm is the probability of asserting the presence of a target when the target is actually absent:

$$P_{\mathrm{fa}} = \int_{R_0}^{\infty} p(r|H_0)\, dr \tag{14}$$

A sketch of the two density functions is shown in Fig. 5, where P_{d} and P_{fa} are, respectively, shown by the vertically and the horizontally hatched areas. If the observed value r is large, we would be confident in picking H_1. If r is small, we would pick H_0, as shown in Fig. 5.

Obviously, a decision rule should be selected to maximize P_{d} while restricting the P_{fa}. The simplest rule in this class, which is extensively used in radar detection, is the *Neyman-Pearson criterion*. This criterion specifies a decision boundary that maximizes the probability of detection (P_{d}) while maintaining a fixed probability of

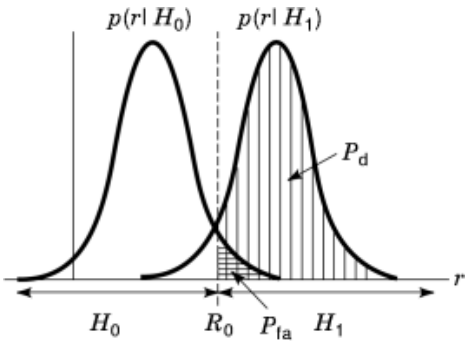

Fig. 5. Probability of false alarm P_{fa} and probability of detection P_d, which are functions of the threshold R_0.

false alarm P_{fa}. The detection problem under the Neyman–Pearson criterion can be formulated as follows:

$$\begin{aligned} \text{Maximum:} \quad & P_d = \int_{R_0}^{\infty} p(r|H_1)\,dr \\ \text{Under constraint:} \quad & P_{fa} = \int_{R_0}^{\infty} p(r|H_0)\,dr = \alpha \end{aligned} \tag{15}$$

The optimum decision region can be found by using the calculus of extrema and forming the objective function

$$J = P_d + \eta(\alpha - P_{fa}) \tag{16}$$

where η is a Lagrange multiplier. This can be written as

$$J = \eta\alpha + \int_{R_0}^{\infty} [p(r|H_1) - \eta p(r|H_0)]\,dr \tag{17}$$

The integration interval in Eq. (17) is related to choosing the hypothesis H_1, as illustrated in Fig. 5. It is clear that J and hence P_d are maximized by choosing the hypothesis H_1 when

$$p(r|H_1) - \eta p(r|H_0) > 0 \tag{18}$$

and by choosing the hypothesis H_0 when

$$p(r|H_1) - \eta p(r|H_0) < 0 \tag{19}$$

To this end, the decision rule based on the Neyman–Pearson criterion is

$$\Lambda(r) \underset{H_0}{\overset{H_1}{\gtrless}} \eta \tag{20}$$

and η is determined by the required false alarm probability α. In radar detection, the choice of α is based upon operational considerations, that is, the need to keep the false alarm rate within acceptable bounds (e.g., a few false alarms per second). A typical value of α for radar detection is 10^{-6}.

Other popular criteria are the *Bayes criterion* and the *minimum error probability* (*MEP*) *criterion.* The Bayes criterion minimizes the average cost of the decision. Symbols denoted by C_{00}, C_{01}, C_{10}, and C_{11} represent the costs for a correct miss (no target is declared when no target is present), a false dismissal (no target is declared when a target is present), a false alarm, and a correct detection, respectively. Also denoted are the *a priori* probabilities $P(H_0)$ and $P(H_1)$ by P_0 and P_1, respectively. The Bayes rule makes the likelihood ratio test

$$\Lambda(r) \underset{H_0}{\overset{H_1}{\gtrless}} \eta \tag{21}$$

where $\eta = [P_0(C_{10} - C_{00})]/[P_1(C_{01} - C_{11})]$. If we select the cost of an error to be 1 and the cost of a correct decision to be 0, $C_{01} = C_{10} = 1$, and $C_{00} = C_{11} = 0$. In this case, minimizing the average cost is equivalent to minimizing the probability of error. Therefore, the MEP rule is the same as expression Eq. (21), but with $\eta = P_0/P_1$. If the *a priori* probabilities are equal, that is, $P_0 = P_1$, the MEP rule coincides with the ML rule with $\eta = 1$.

Implementation of Decision Criteria

Let us suppose that the observed signal r has the following Gaussian distribution conditional probability density functions,

$$p(r|H_0) = \frac{1}{\sqrt{2\pi}\sigma} e^{r^2/(2\sigma^2)} \tag{22}$$

$$p(r|H_0) = \frac{1}{\sqrt{2\pi}\sigma} e^{(r-\mu)^2/(2\sigma^2)} \tag{23}$$

where μ denotes the mean of the received signal value and σ^2 represents the noise variance. The likelihood ratio test is therefore

$$\Lambda(r) = \frac{e^{(r-\mu)^2/(2\sigma^2)}}{e^{r^2/(2\sigma^2)}} \underset{H_0}{\overset{H_1}{\gtrless}} \eta \tag{24}$$

After taking the logarithm of both sides, the criterion becomes

$$R_0 \underset{H_0}{\overset{H_1}{\gtrless}} \frac{\sigma^2}{\mu} \ln \eta + \frac{\mu}{2} \tag{25}$$

In Eq. (25) it is seen that the likelihood ratio test, in which $\Lambda(r)$ of Eq. (24) is compared with a threshold η, is transformed into a comparison of the observable r with the threshold in Eq. (25), which is a function of η. As an example, supposing $P(H_0)$ and $P(H_1)$ are known, with $P(H_0)/P(H_1) = 2$, then the decision rules are choose H_1 if

$$\text{for the maximum likelihood } (\eta = 1), \qquad R_0 > \frac{\mu}{2} \tag{26}$$

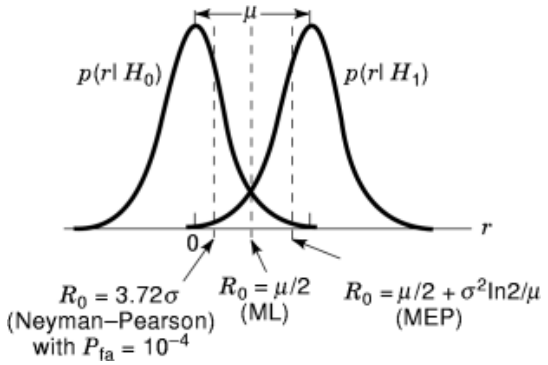

Fig. 6. Decision thresholds for different decision criteria.

$$\text{for the minimum error probability } (\eta = 2), \quad R_0 > \frac{\mu}{2} + \frac{\sigma^2 \ln 2}{\mu} \tag{27}$$

Since the a priori probability of H_0 is twice that of H_1, the MEP rule requires a larger value of R_0 for the selection of H_0 than the ML, in which this information is not used. The MEP scheme therefore yields a better decision rule in this case.

For a Neyman–Pearson criterion, suppose a value of $P_{\text{fa}} = 10^{-4}$ can be tolerated. The threshold η is determined from

$$P_{\text{fa}} = 10^{-4} = \int_{R_0}^{\infty} \frac{1}{\sqrt{2\pi}\sigma} e^{-x^2/(2\sigma^2)}\, dx \tag{28}$$

to be $\eta = 3.72\sigma$. So H_1 is chosen if

$$\text{for the Neyman–Pearson rule } (P_{\text{fa}} = 10^{-4}), \quad R_0 > 3.72\sigma \tag{29}$$

A typical illustration of these thresholds for this example's three decision criteria is given in Fig. 6. An important observation is that these criteria employ the likelihood ratio test. In other words, the test is performed by simply processing the received data to yield the likelihood ratio and then comparing it with the threshold, which depends upon the criterion used. Thus, in practical situations where the a priori probabilities and the cost may vary, only the threshold changes, and the computation of the likelihood ratio is not affected.

As observed previously, in radar detection it is very hard to define the Bayes cost C_{ij}; moreover, it is also practically impossible to define or evaluate the a priori probabilities P_0 and P_1, that is, the probabilities that, in a given resolution interval, a target is present or absent. These are the main reasons why the Bayes and minimum error probability criteria cannot be used in radar detection. In contrast, for the same reason, the Neyman–Pearson criterion is particularly well suited to radar detection, owing to its concept of the "P_{fa} threshold" fixed a priori, while P_{d} is maximized.

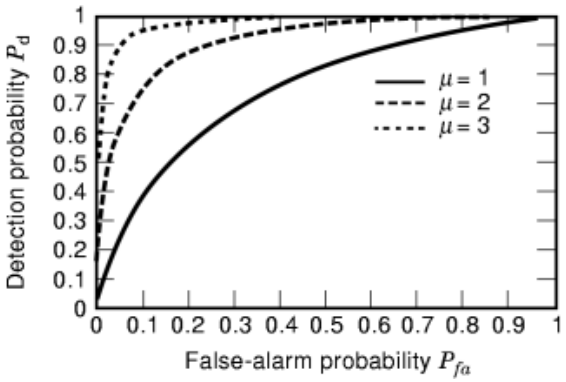

Fig. 7. ROC curves for different values of μ.

Receiver Operating Characteristic

A graph showing the probability of detection, P_d, versus the probability of false alarm, P_{fa}, with the threshold as a parameter is referred to as a receiver operating characteristic (*ROC*) curve. We note that the ROC depends on the conditional density function of the observed signal under each hypothesis, that is, $p(r|H_i)$, $i = 0, 1$, and not on the assigned costs, or a priori probabilities.

Suppose that the observed signal r has the probability density functions of Eqs. (22) and (23). Varying the threshold R_0, P_d of Eq. (13), and P_{fa} of Eq. (14) produces the corresponding ROC curves for $\sigma = 1$ and $\mu = 1, 2, 3$ as shown in Fig. 7.

The two extreme points on the ROC for $P_{fa} = P_d = 1$ and $P_{fa} = P_d = 0$ are easily verified. P_d of Eq. (13) may be rewritten as a function of the likelihood ratio $\Lambda(r)$ as

$$P_d = \int_{\eta}^{\infty} p_{\Lambda}(\lambda|H_1)\, d\lambda \tag{30}$$

where η is the threshold of the likelihood ratio just as R_0 is the threshold of the observed signal, and $p_{\Lambda}(\lambda|H_1)$ in Eq. (30) is the conditional probability density function of the variable Λ. Similarly, P_{fa} of Eq. (14) is rewritten as

$$P_{fa} = \int_{\eta}^{\infty} p_{\Lambda}(\lambda|H_0)\, d\lambda \tag{31}$$

Since Λ is a ratio of two non-negative quantities, it takes on values from 0 to ∞. When the threshold η is 0, the hypothesis H_1 is always true and thus $P_{fa} = P_d = 1$. When the threshold η is ∞, the hypothesis H_0 is always true and thus $P_{fa} = P_d = 0$. These are clearly depicted in Fig. 7.

Of course, ROC curves may be drawn for any hypothesis test involving a threshold, but the ROC curves have particularly useful properties for the likelihood ratio test. One is the fact that the slope of the ROC at a particular point on the curve represents the threshold value of the likelihood ratio η. Taking the derivative of Eqs. (30) and (31) with respect to η, we have

$$\frac{dP_d}{d\eta} = -p_{\Lambda}(\eta|H_1) \tag{32}$$

and

$$\frac{dP_{\text{fa}}}{d\eta} = -p_{\Lambda}(\eta|H_0) \tag{33}$$

Also,

$$\begin{aligned} P_{\text{d}} &= \int_{R_0}^{\infty} \Lambda(r) p(r|H_0)\, dr \\ &= \int_{\eta}^{\infty} \lambda p_{\Lambda}(\lambda|H_0)\, d\lambda \end{aligned} \tag{34}$$

Taking the derivative of Eq. (34) with respect to η, we obtain

$$\frac{dP_{\text{d}}}{d\eta} = -\eta p_{\Lambda}(\eta|H_0) \tag{35}$$

Combining Eqs. (32), (33), and (35), the slope of the ROC curve obtained is

$$\frac{dP_{\text{d}}}{dP_{\text{fa}}} = \frac{p_{\Lambda}(\eta|H_1)}{p_{\Lambda}(\eta|H_0)} = \eta \tag{36}$$

In the Neyman–Pearson criterion, the slope of the ROC curve at a particular point represents the likelihood ratio threshold η of achieving P_{d} and P_{fa} at that point. In the Bayes criterion, the threshold η is determined by a priori probabilities and the costs. Consequently, P_{d} and P_{fa} are determined on the point of the ROC at which the tangent has a slope of η.

Since the ROC curves are always concave and facing downward, it is possible to determine an "optimum" value (the knee) for P_{fa}, such that a small decrease of its value causes a fast decrease of P_{d}, while any increase has a very small effect (the saturation zone, where the rate of change is nearly 0).

Finally, we note that the most important part of the ROC curve is the upper left-hand (northwest) corner. This is the so-called high-performance corner, where a high-detection probability occurs with a low false-alarm probability. This part of the plot could be stretched out by the use of appropriate (such as logarithmic) scales.

Analysis of a Matched Filter

Derivation of the Matched Filter. The matched filter achieves the maximum output SNR, which is

$$\frac{S}{N} = \frac{(\text{maximum instantaneous output signal power})}{(\text{output noise power})} \tag{37}$$

Consider a signal $s(t)$ with the spectrum $S(f)$ and finite energy

$$E_s = \int_{-\infty}^{\infty} |s(t)|^2\, dt = \int_{-\infty}^{\infty} |S(f)|^2\, df \tag{38}$$

For the input signal $s(t)$ and the filter with transfer function $H(f)$, the instantaneous power of the output signal $y(t)$ is

$$|y(t)|^2 = \left| \int_{-\infty}^{\infty} S(f)H(f)e^{j2\pi ft} df \right|^2 \tag{39}$$

For white noise with a two-sided noise power spectral density $N_0/2$, the output power spectral density is $|H(f)|^2 N_0/2$. Therefore, the noise power at the filter output is

$$\sigma^2 = \frac{N_0}{2} \int_{-\infty}^{\infty} |H(f)|^2 \, df \tag{40}$$

Using Eqs. (39) and (40) in Eq. (37) in leads to the following:

$$\frac{S}{N} = \frac{|\int_{-\infty}^{\infty} S(f)H(f)e^{j2\pi fT} df|^2}{(N_0/2)\int_{-\infty}^{\infty} |H(f)|^2 \, df} \tag{41}$$

where T denotes the time at which the maximum value of $|y(t)|^2$ occurs.

Using Schwarz's inequality

$$\left| \int_{-\infty}^{\infty} f(x)g(x) \, dx \right|^2 \leq \int_{-\infty}^{\infty} |f(x)|^2 \, dx \int_{-\infty}^{\infty} |g(x)|^2 \, dx \tag{42}$$

we obtain

$$\frac{S}{N} \leq \frac{\int_{-\infty}^{\infty} |S(f)|^2 \, df \int_{-\infty}^{\infty} |H(f)|^2 \, df}{(N_0/2)\int_{-\infty}^{\infty} |H(f)|^2 \, df} \tag{43}$$

It follows that the signal-to-noise ratio will be a maximum when

$$H(f) = kS^*(f)e^{-j2\pi fT} \tag{44}$$

yielding the requirement of the matched filter. From discussions above it is evident that the maximum signal-to-noise ratio can be expressed as

$$\text{SNR}|_{\max} = \frac{2E_s}{N_0} \tag{45}$$

Equation (45) indicates that the detection capability of a particular signal depends only on its energy content, and not on the time structure of the signal. However, it is necessary to process the signal through a matched filter to obtain this condition in practice. We note that E_s/N_0 is defined as the input SNR, and it is clear from Eq. (45) that the maximum output SNR for the matched filter is twice that of the input SNR if the noise is white.

In general case, when the noise is nonwhite (colored noise), the derivation of the matched filter can be carried out in a similar way. If the power spectral density of the nonwhite noise is $N(f)$, then Eq. (40) is written as

$$\sigma^2 = \int_{-\infty}^{\infty} N(f)|H(f)|^2\,df \tag{46}$$

Therefore, by multiplying and dividing the integrand of the numerator of Eq. (41) by $\sqrt{N(f)}$ and using Eq. (46):

$$\begin{aligned}\frac{S}{N} &= \frac{\left|\int_{-\infty}^{\infty} \frac{S(f)}{\sqrt{N(f)}} H(f)\sqrt{N(f)}e^{j2\pi fT}\,df\right|^2}{\int_{-\infty}^{\infty} N(f)|H(f)|^2\,df} \\ &\le \frac{\int_{-\infty}^{\infty} |S(f)|^2/N(f)\,df \int_{-\infty}^{\infty} |H(f)|^2 N(f)\,df}{\int_{-\infty}^{\infty} |H(f)|^2 N(f)\,df} \\ &= \int_{-\infty}^{\infty} |S(f)|^2/N(f)\,df\end{aligned} \tag{47}$$

and the maximum is achieved when

$$H(f) = \frac{kS^*(f)e^{-j2\pi fT}}{N(f)} \tag{48}$$

The conjugate is not needed in the denominator because $N(f)$ is always real (and nonnegative). If the noise is white—that is, if $N(f)$ is a constant over the band of $H(f)$—then Eq. (48) is the same as Eq. (44) for the white noise. The matched filter for nonwhite noise can be interpreted as the cascade of two filters. The first one, whose transfer function is $1/\sqrt{N(f)}$ is the "whitening" filter. This filter makes the noise spectrum flat (white). The second one is matched to the signal filtered by the whitening filter, that is, to the whitening signal with the spectrum $S(f)/\sqrt{N(f)}$.

We note that it is not necessary that the noise be Gaussian for Eq. (45) to hold, but only that its power spectral density be flat over the frequency band of interest. To summarize, the matched filter maximizes the output SNR over all probability densities, provided the power spectral density (*PSD*) is a constant. In the event that the noise PSD is nonwhite (colored noise), the matched impulse response corresponds to the modified signal spectrum $S*(f)e^{-j2\pi fT}/\sqrt{N(f)}$ rather than simply $S*(f)e^{-j2\pi fT}$.

Justification of the Signal-to-Noise Ratio Criterion. We derived the matched filter under the criterion of maximizing the output SNR. We remark here that the matched filter can also be derived under the likelihood ratio criterion (1). In this section, we want to justify the maximum output SNR criterion, and more specifically derive the relationship between the output SNR and the system performance in terms of the probability of error.

The total probability of error for a radar receiver consists of the false-alarm probability P_{fa} and the false-dismissal probability P_{fd}. A false dismissal declares no target when a target is present, that is,

$$P_{\text{fd}} = \int_{-\infty}^{R_0} p(r|H_1)\,dr \tag{49}$$

For equal a priori probabilities $P(H_0) = P(H_1) = 1/2$, the total probability of error is

$$\begin{aligned} P_{\text{e}} &= \tfrac{1}{2}(P_{\text{fd}} + P_{\text{fa}}) \\ &= \tfrac{1}{2} + \tfrac{1}{2}\int_{-\infty}^{R_0}[p(r|H_1) - p(r|H_0)]\,dr \end{aligned} \tag{50}$$

Supposing $p(r|H_i)$, $i = 0, 1$ is a Gaussian distribution that is given by Eqs. (22) and (23), P_{e} can be expressed as

$$\begin{aligned} P_{\text{e}} &= \frac{1}{2} - \frac{1}{2}\left(\frac{1}{\sqrt{\pi}}\int^{(\mu - R_0)/\sqrt{2}\sigma} e^{-r^2}\,dr + \frac{1}{\sqrt{\pi}}\int_0^{\frac{R_0}{\sqrt{2}\sigma}} e^{-r^2}\,dr\right) \\ &= \frac{1}{2} - \frac{1}{4}\left[\text{erf}\left(\frac{\mu - R_0}{\sqrt{2}\sigma}\right) + \text{erf}\left(\frac{R_0}{\sqrt{2}\sigma}\right)\right] \end{aligned} \tag{51}$$

where

$$\text{erf}(x) = \frac{2}{\pi}\int_0^x e^{-r^2}\,dr \tag{52}$$

is the error function. The minimum of P_{e} occurs when $R_0 = \mu/2$, and

$$P_{\text{e}}\big|_{\min} = \tfrac{1}{2}\text{erfc}\left(\frac{\mu/2}{\sqrt{2}\sigma}\right) \tag{53}$$

where

$$\text{erfc}(x) = 1 - \text{erf}(x) = \frac{2}{\sqrt{\pi}}\int_x^\infty e^{-r^2}\,dr \tag{54}$$

is the complementary error function. Recalling that μ is the expectation of the matched filter output at time T under the H_1 hypothesis

$$\mu = E[y(T)|H_1] = E\left[\int_0^T [s(\tau) + n(\tau)]s(\tau)\,d\tau\right] = E_{\text{s}} \tag{55}$$

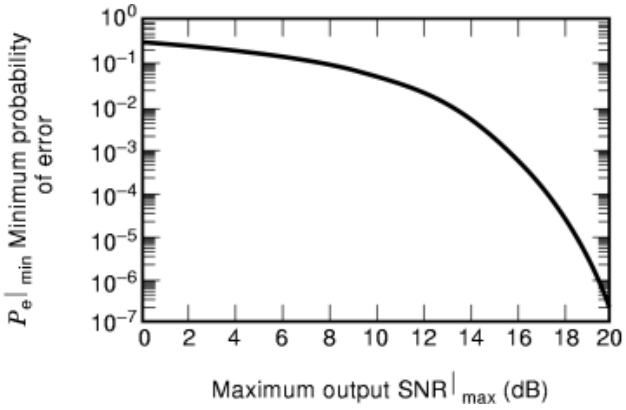

Fig. 8. Minimum error probability $P_e|_{min}$ versus maximum output signal-to-noise ratio $SNR|_{max}$.

and

$$E[y(T)|H_0] = E\left[\int_0^T n(\tau)s(\tau)\,d\tau\right] = 0 \tag{56}$$

Defining σ^2 to be the variance of $y(T)$ under the H_0 or H_1 hypotheses, it is given that

$$\begin{aligned}\sigma^2 &= \mathrm{Var}[y(T)|H_1] = \mathrm{Var}[y(T)|H_0] \\ &= \int_0^T \int_0^T E[n(t)n(\tau)]s(t)s(\tau)\,dt\,d\tau \\ &= \frac{N_0}{2}\int_0^T \int_0^T \delta(t-\tau)s(t)s(\tau)\,dt\,d\tau \\ &= \tfrac{1}{2}E_s N_0\end{aligned} \tag{57}$$

The application of Eqs. (55) and (57) to Eq. (53) leads to the following minimum probability of error:

$$\begin{aligned}P_e|_{\min} &= \tfrac{1}{2}\mathrm{erfc}\left(\sqrt{\frac{E_s}{4N_0}}\right) \\ &= \tfrac{1}{2}\mathrm{erfc}\left(\sqrt{\frac{\mathrm{SNR}|_{\max}}{8}}\right)\end{aligned} \tag{58}$$

It is clear from Eq. (58) that $P_e|_{min}$ is inversely proportional to $SNR|_{max}$, because $\mathrm{erfc}(x)$ is a monotonic decreasing function. In other words, a lower probability of error means a higher output SNR, and requires a higher input SNR. Figure 8 shows the relationship between $P_e|_{min}$ and $SNR|_{max}$. This curve should be shifted to the left by 3 dB if it is plotted with respect to the input SNR, since $SNR|_{max}$ is twice the input SNR. For example, a 10^{-5} error probability corresponds to an output SNR of 18.6 dB, and 15.6 dB of input SNR is required. Therefore, it is justifiable to use the signal-to-noise ratio criterion in radar detection.

Noncoherent Detections

A received radar signal is a *bandpass* random process because it is modulated on a carrier. Radar detection is classified into coherent and noncoherent detections depending upon whether the carrier phase at the receiver is available. Specifically, the matched filter and the cross-correlation discussed previously are coherent because they require the knowledge of the carrier phase. The envelope and all the other nonlinear detections are noncoherent due to their ignorance of the phase information in the received signal. To understand the nonlinear detections, we introduce the representations of bandpass signals and bandpass processes.

Representation of Band-Pass Signals. The concept of a band-pass signal is a generalization of the concept of monochromatic signals. A bandpass signal is a signal $x(t)$ whose spectrum $X(f)$ is nonzero for frequencies in a usually small neighborhood of some high frequency f_0, that is,

$$X(f) = 0 \quad \text{for} \quad |f - f_0| \geq W \tag{59}$$

where the frequency f_0 is referred to as the central frequency (carrier frequency) of the bandpass signal. A radar signal that is modulated on a carrier is a bandpass signal. It is assumed that the band-pass signal is real-valued. Figure 9(a) illustrates the spectrum of a bandpass signal $x(t)$. A real-valued bandpass signal $x(t)$ can be represented as the real part of a complex signal $x_+(t)$, called the *preenvelope* or *analytic signal* of $x(t)$, where

$$x_+(t) = x(t) + j\hat{x}(t) \tag{60}$$

and

$$\hat{x}(t) = \frac{1}{\pi} \int_{-\infty}^{\infty} \frac{x(\tau)}{t - \tau} d\tau \tag{61}$$

is the Hilbert transform of $x(t)$. The spectrum of the preenvelope signal is readily found from the Fourier transform of Eq. (60) to be

$$X_+(f) = X(f) + X(f)\text{sgn}(f) = \begin{cases} 2X(f), & f > 0 \\ X(0), & f = 0 \\ 0, & f \leq 0 \end{cases} \tag{62}$$

The spectrum of the preenvelope signal is obtained by deleting the negative frequencies from $X(f)$ and multiplying the positive frequencies in $X(f)$ by two, as illustrated in Fig. 9(b).

The spectrum of the *complex envelope* is obtained by shifting $X_+(f)$ to the left by f_0, that is,

$$\tilde{X}(f) = X_+(f + f_0) \tag{63}$$

and

$$\tilde{x}(t) = x_+(t)e^{-j2\pi f_0 t} \tag{64}$$

The amplitude spectrum of $\tilde{x}(t)$ is illustrated in Fig. 9(c).

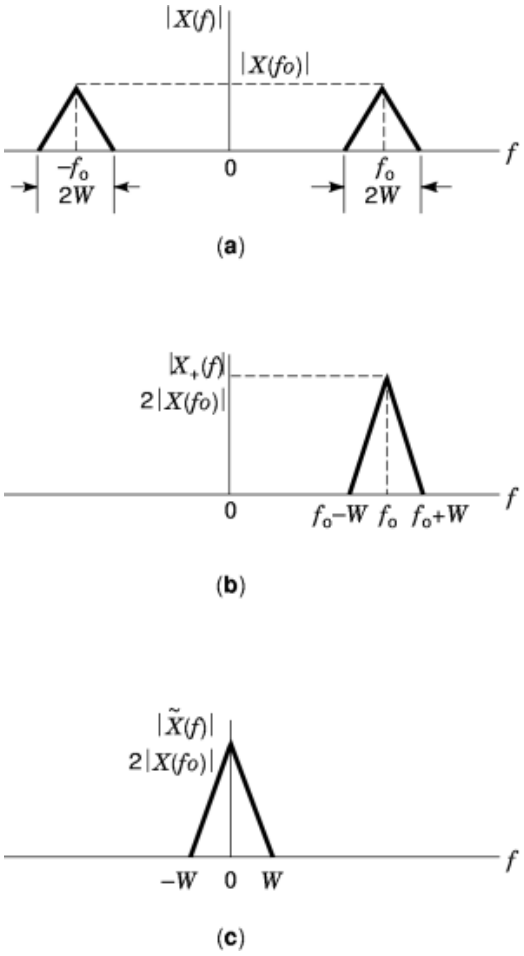

Fig. 9. (a) Amplitude spectrum of a band-pass signal $x(t)$. (b) Amplitude spectrum of preenvelope $x_+(t)$. (c) Amplitude spectrum of complex envelope $\tilde{x}(t)$. The spectrum of $x_+(t)$ is twice the positive spectrum of $x(t)$, and the spectrum of $\tilde{x}(t)$ is a low-pass version of that $x_+(t)$.

It is clear that $\tilde{x}(t)$ is a low-pass signal, meaning that its frequency components are located around the zero frequency. $\tilde{x}(t)$ is the low-pass representation of the bandpass signal $x(t)$. In general, $\tilde{x}(t)$ is a complex signal having $x_c(t)$ and $x_s(t)$ as its real and imaginary parts:

$$\tilde{x}(t) = x_c(t) + jx_s(t) \tag{65}$$

where $x_c(t)$ and $x_s(t)$ are low-pass signals, respectively, and are called the *in-phase* and *quadrature* components of the bandpass signal $x(t)$. Notice that $x(t)$ is the real part of $x_+(t)$. Using Eq. (65), we obtain

$$\begin{aligned} x(t) &= \mathrm{Re}[\tilde{x}(t)e^{j2\pi f_0 t}] \\ &= x_c(t)\cos(2\pi f_0 t) - x_s(t)\sin(2\pi f_0 t) \end{aligned} \tag{66}$$

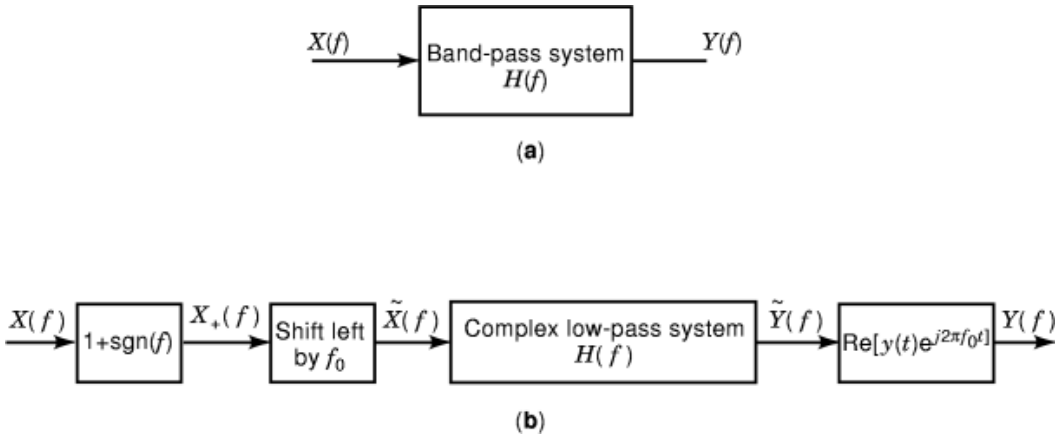

Fig. 10. (a) Band-pass description and (b) complex envelope description of a system. Complex envelope description simplifies the analysis of a bandpass signal.

This is the *canonical representation* for a bandpass signal in terms of the in-phase component $x_c(t)$ and quadrature component $x_s(t)$ of the complex envelope associated with the signal.

The complex envelope can be employed to find the outputs of bandpass systems driven by bandpass signals. Accordingly, by analyzing the complex envelope representation of a band-pass signal, we may develop the complex low-pass representation of the bandpass system by retaining the positive-frequency half of the transfer function $H(f)$, and shift it to the left by f_0. Let $\tilde{H}(f)$ denote the transfer function of the complex low-pass system so defined. The analysis of the bandpass system with transfer function $H(f)$ driven by the bandpass signal with spectrum $X(f)$, as depicted in Fig. 10(a), is replaced by an equivalent but simpler analysis of a complex low-pass system with transfer function $\tilde{H}(f)$ driven by a complex low-pass input with spectrum $\tilde{X}(f)$, as shown in Fig. 10(b). The complex low-pass output $\tilde{y}(t)$ is obtained from the inverse Fourier transform of $\tilde{Y}(f)$. Having determined $\tilde{y}(t)$, we may find the desired band-pass output $y(t)$ simply by using the relation

$$y(t) = \mathrm{Re}[\tilde{y}(t)e^{j2\pi f_0 t}] \tag{67}$$

The bandpass to low-pass transformation is also true for bandpass random processes. $X(t)$ is a bandpass process if its power spectral density $S_x(f) = 0$ for $|f - f_0| \geq W$. $X(t)$ can be represented by its in-phase component $X_c(t)$ and quadrature component $X_s(t)$ in the same way that a bandpass signal does. Specifically,

$$X(t) = X_c(t)\cos(2\pi f_0 t) - X_s(t)\sin(2\pi f_0 t) \tag{68}$$

where $X_c(t)$ and $X_s(t)$ are two low-pass processes representing the real and imaginary parts of the complex envelope process $\tilde{X}(t)$, respectively. $X(t)$ can be found from the complex envelope process $\tilde{X}(t)$ by

$$X(t) = \mathrm{Re}[\tilde{X}(t)e^{j2\pi f_0 t}] \tag{69}$$

Envelope Detection and Square-Law Detection. The matched filter is the optimal detection for an exactly known signal (i.e., phase, amplitude, and Doppler frequency are known) in a background of white noise. However, both the matched filter and the cross-correlation need to generate a synchronous reference, which

is difficult to realize. In a typical radar application, the range between the target and the radar represents a very large number of transmitted signal wavelengths. This makes specifying the phase of the return signal extremely difficult, and we usually assume that the signal phase of the return signal is a random variable uniformly distributed over an angle of 2π rad. The matched-filter detection is often used to set a standard of performance, as it represents the optimal detection when all signal parameters are exactly known.

The synchronization problem in the matched-filter detection is obviated in a practical system by employing an envelope detection. The envelope $V(t)$ of a bandpass signal $x(t)$ is given by

$$V(t) = \sqrt{x_s^2(t) + x_c^2(t)} \tag{70}$$

The complex envelope $\tilde{x}(t)$ can be represented more compactly as

$$\tilde{x}(t) = V(t)e^{j\theta(t)} \tag{71}$$

where

$$\theta(t) = \arctan\frac{x_s(t)}{x_c(t)} \tag{72}$$

The procedure for obtaining the envelope is shown in Fig. 11, which is the extraction of the in-phase and quadrature components and the derivation of the envelope from them. Specifically, the multiplication of $x(t)$ by $2\cos(2\pi f_0 t)$ in the in-phase channel yields

$$\begin{aligned} 2x(t)\cos(2\pi f_0 t) &= 2\cos(2\pi f_0 t)[x_c(t)\cos(2\pi f_0 t) \\ &\quad - x_s(t)\sin(2\pi f_0 t)] \\ &= x_c(t) + x_c(t)\cos(4\pi f_0 t) - x_s(t)\sin(4\pi f_0 t) \end{aligned} \tag{73}$$

The mixing operation produces two images besides the expected low-pass component. The product $2x(t)\cos(2\pi f_0 t)$ is passed through an ideal low-pass filter (the integrator in Fig. 11), which rejects the images and leaves $x_c(t)$. Similar operations in the quadrature channel produce $x_s(t)$. The square sum of the quadrature components yields the envelope $V(t)$.

Removing the square-root operation from Fig. 11 yields the square-law detection. A detailed performance analysis of these detections is given in the section entitled "Performance Analysis of Coherent and Noncoherent Detections."

The envelope can be extracted alternatively by passing the band-pass signal $x(t)$ through a rectifier and a low-pass filter, as illustrated in Fig. 12. Such a description can sometimes simplify the analysis and is easier to implement physically because the various rectifiers are readily available from the diodes and the transistors. The output of the full-wave linear rectifier is proportional to the magnitude of its input, while the output of the full-wave square-law (quadratic) rectifier is proportional to the squared magnitude of its input. The half-wave rectifier, of course, gives only the positive portion of its input. Fig. 13 shows these transfer characteristics. Referring to Fig. 12, we may write

$$V(t) = \mathrm{Env}[x(t)] = \mathrm{LF}[|x(t)|] \tag{74}$$

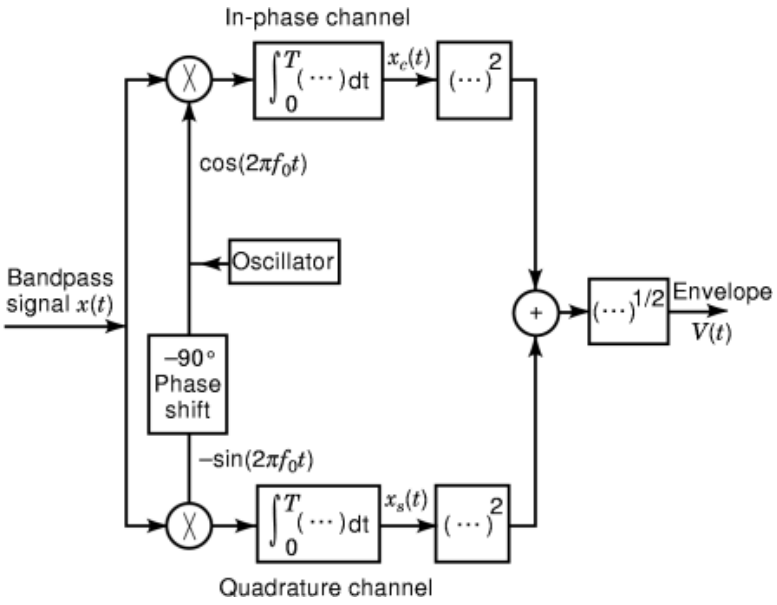

Fig. 11. Block diagram of the envelope detection.

where LF indicates the low-frequency portion. Also, considering the full-wave quadratic rectifier in place of the full-wave linear rectifier, we may write

$$V^2(t) = \mathrm{LF}[x^2(t)] \tag{75}$$

The band-pass signal $x(t)$ in Eqs. (74) and (75) has the following form:

$$x(t) = V(t)\cos[2\pi f_0 t + \theta(t)] \tag{76}$$

Then in the case of the square-law rectifier, we have

$$\begin{aligned} x^2(t) &= V^2(t)\cos^2[2\pi f_0 t + \theta(t)] \\ &= \tfrac{1}{2}V^2(t) + \tfrac{1}{2}V^2(t)\cos[4\pi f_0 t + 2\theta(t)] \end{aligned} \tag{77}$$

Since the envelope $V(t)$ is slowly varying compared to the carrier frequency f_0, the first term in Eq. (77) is concentrated around zero frequency. The fact that the term is the square of the envelope means that the bandwidth will be somewhat greater than that of $V(t)$. The second term in Eq. (77) will be concentrated around $2f_0$ with a bandwidth that depends on both the envelope square $V^2(t)$ and the phase modulation $\theta(t)$. In most cases of interest, the bandwidth of the total modulation will be small enough compared to f_0 so that the low-pass filter following the rectifier will easily separate the low-frequency portion of Eq. (77).

Fig. 12. Envelope detection with a linear rectifier.

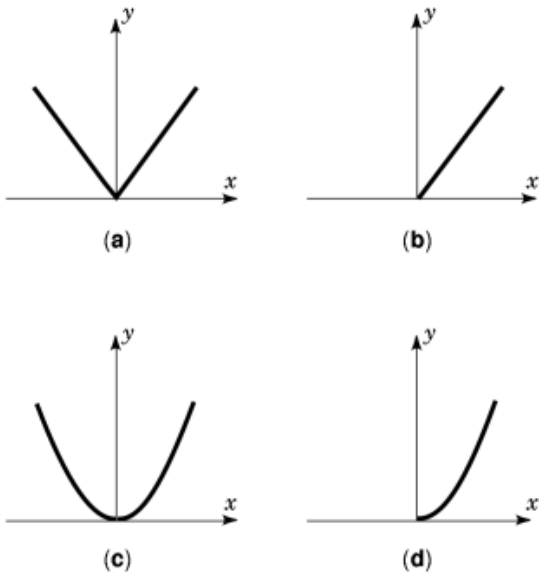

Fig. 13. Various rectifier characteristics for (a) full-wave linear rectifier, (b) half-wave linear rectifier, (c) full-wave square-law (quadratic) rectifier, and (d) half-wave square-law (quadrature) rectifier.

In the case of the full-wave linear rectifier, we may write

$$\begin{aligned} |x(t)| &= V(t)|\cos[2\pi f_0 t + \theta(t)]| \\ &\approx \frac{2V(t)}{\pi}\{1 + \tfrac{2}{3}\cos[4\pi f_0 t + 2\theta(t)] \\ &\quad - \frac{2}{15}\cos[8\pi f_0 t + 4\theta(t)] + \cdots\} \end{aligned} \tag{78}$$

The low-pass filter will remove all of the terms in the curly bracket except for the first term. Thus, if the bandwidth of $V(t)$ is not too large, a very good approximation of the envelope can be obtained. A similar analysis can be carried out to show that the half-wave linear and the half-wave quadratic rectifiers extract the envelope $V(t)$.

We note that the envelope detection is referred to as a linear detection, due to its transfer characteristic stipulating that the output is proportional to the input when the input is positive, as illustrated in Fig. 13(a). The operation of the envelope detection, however, is of course highly nonlinear, and as a result the output consists of a dc term proportional to the envelope, plus an infinite number of harmonics of theinput at $2f_0$, $4f_0$, etc. It is for this reason that the envelope detection must be passed through a low-pass filter, thus eliminating the unwanted harmonics. Similar comments apply to the square-law detection.

Justification of the Noncoherent Detections. The justification of the envelope and the square-law detections by the likelihood ratio criterion is given in this subsection. The radar detection process may include

down-conversion of the carrier frequency to a more manageable intermediate frequency (*IF*). This step, however, is irrelevant to the results we are going to obtain and is therefore omitted.

Consider the signal to be a carrier pulse of the form

$$s(t) = \begin{cases} A\cos(2\pi f_0 t + \theta), & 0 \le t \le T \\ 0, & \text{otherwise} \end{cases} \tag{79}$$

The two hypotheses are

$$\begin{aligned} H_1: &\quad r(t) = s(t) + n(t) = A\cos(2\pi f_0 t + \theta) + n(t) \\ H_0: &\quad r(t) = n(t) \end{aligned} \tag{80}$$

for $0 \le t \le T$, and $n(t)$ is a Gaussian white-noise process with two-sided spectral density $N_0/2$.

The detection problem described by Eq. (79) consists of examining the received waveform $r(t)$ and determining whether it consists of a signal plus noise or noise alone. The optimal detection, as previously described, forms the likelihood ratio which is compared against a threshold.

The sampling bandwidth B, which is the reciprocal of the sampling interval, must be sufficiently large to pass along essentially all of the signal energy, which will be the case if $B \ge 1/T$. In this case, by the sampling theorem we know that the number of samples k is given by $k = 2BT$. Given these conditions, the likelihood ratio can be written as

$$\begin{aligned} \Lambda(r) &= \frac{\exp\left(-(1/2\sigma^2)\sum_{i=1}^{2BT}[r(t_i) - s(t_i)]^2\right)}{\exp\left(-(1/2\sigma^2)\sum_{i=1}^{2BT} r^2(t_i)\right)} \\ &= \exp\left(\frac{1}{2\sigma^2}\sum_{i=1}^{2BT}[2r(t_i)s(t_i) - s^2(t_i)]\right) \end{aligned} \tag{81}$$

where the noise variance σ^2 is $(N_0/2)2B = N_0 B$. Recall from the sampling theorem (2,3) that for any two band-limited functions $u(t)$ and $v(t)$ we can write

$$\begin{aligned} &\int_{-\infty}^{-\infty} u(t)v(t)\,dt \\ &\quad = \sum_n \sum_m u\left(\frac{n}{2B}\right) v\left(\frac{m}{2B}\right) \int_{-\infty}^{-\infty} \frac{\sin 2\pi B(t - n/2B)}{2\pi B(t - n/2B)} \\ &\qquad \frac{\sin 2\pi B(t - m/2B)}{2\pi B(t - m/2B)}\,dt \\ &\quad = \frac{1}{2B}\sum_{n=-\infty}^{\infty} u\left(\frac{n}{2B}\right) v\left(\frac{n}{2B}\right) \end{aligned} \tag{82}$$

Applying this to Eq. (81), we have

$$\begin{aligned}\Lambda(r) &= \exp\left(\frac{1}{N_0}\int_0^T [2r(t)s(t) - s^2(t)]dt\right) \\ &= \exp\left(\frac{1}{N_0}\int_0^T [2r(t)A\cos(2\pi f_0 t + \theta) \right. \\ &\qquad \left. - A^2\cos^2(2\pi f_0 t + \theta)]dt\right)\end{aligned} \tag{83}$$

Because the signal is of finite duration, the approximation in passing from the discrete to the continuous representation improves as B is allowed to become very large.

In the noncoherent case, θ in Eq. (83) is unknown. Since no auxiliary information about θ is available, it is reasonable to assume θ to be uniformly distributed over 2π rad. An average likelihood ratio is

$$\begin{aligned}\Lambda(r)_{\text{av}} &= \int_0^{2\pi} \Lambda(r)p(\theta)d\theta \\ &= \frac{\exp(-A^2T/2N_0)}{2\pi}\int_0^{2\pi} \\ &\qquad \left[\exp\left(-\frac{2A}{N_0}\int_0^T r(t)\cos(2\pi f_0 t + \theta)\,dt\right)\right]\end{aligned} \tag{84}$$

The exponent in the integrand can be written as

$$\begin{aligned}&-\frac{2A}{N_0}\int_0^T r(t)\cos(2\pi f_0 t + \theta)\,dt \\ &= -\frac{2A}{N_0}X_c\cos\theta + \frac{2A}{N_0}X_s\sin\theta\end{aligned} \tag{85}$$

where

$$X_c = \int_0^T r(t)\cos(2\pi f_0 t)\,dt, \quad X_s = \int_0^T r(t)\sin(2\pi f_0 t)\,dt \tag{86}$$

and Eq. (84) becomes

$$\begin{aligned}\Lambda(r)_{\text{av}} &= \exp\left(-\frac{A^2T}{2N_0}\right)\int_0^{2\pi}\exp\left(-\frac{2A}{N_0}(X_c\cos\theta - X_s\sin\theta)\right)\frac{d\theta}{2\pi} \\ &= \exp\left(-\frac{A^2T}{2N_0}\right)I_0\left(\frac{2AV}{N_0}\right)\end{aligned} \tag{87}$$

where $V = \sqrt{X_c^2 + X_s^2}$ and I_0 is the modified Bessel function of order zero. The likelihood ratio test is therefore

$$\ln\left[I_0\left(\frac{2AV}{N_0}\right)\right] \underset{H_0}{\overset{H_1}{\gtrless}} (E_s/N_0)\eta \tag{88}$$

where the signal energy $E_s = A^2T/2$. Thus the natural logarithm of the modified Bessel function I_0 is the optimum noncoherent detection characteristic. For a large SNR, the likelihood ratio test can be approximated as

$$\ln\left[I_0\left(\frac{2AV}{N_0}\right)\right] \approx \frac{2AV}{N_0} \underset{H_0}{\overset{H_1}{\gtrless}} (E_s/N_0)\eta \tag{89}$$

and for a small SNR,

$$\ln\left[I_0\left(\frac{2AV}{N_0}\right)\right] \approx \frac{A^2V^2}{2N_0^2} \underset{H_0}{\overset{H_1}{\gtrless}} (E_s/N_0)\eta \tag{90}$$

The implementation of the likelihood ratio test of Eq. (89) has been shown in Fig. 11, where the in-phase and the quadrature channels generate the x_c and x_s in Eq. (86), respectively. Summation of the square of x_c and x_s yields the square-law detection of Eq. (90). Taking the square root in addition to the square-law detection yields the envelope detection of Eq. (89).

Performance Analysis of Coherent and Noncoherent Detections

Detection Probability Analysis. From the mean and the variances given by Eqs. (55) to (57), the false-alarm probability P_{fa} for the coherent detection is determined by

$$\begin{aligned} P_{fa} &= \int_{R_0}^{\infty} \frac{1}{\sqrt{\pi E_s N_0}} \exp^{(-x^2/E_s N_0)}\, dx \\ &= \frac{1}{\sqrt{\pi}} \int_{R_0/\sqrt{E_s N_0}}^{\infty} e^{-x^2}\, dx \\ &= \frac{1}{2}\operatorname{erfc}\left(\frac{R_0}{\sqrt{E_s N_0}}\right) \end{aligned} \tag{91}$$

The detection probability P_d is given by

$$\begin{aligned} P_d &= \int_{R_0}^{\infty} \frac{1}{\sqrt{\pi E_s N_0}} \exp^{(-(x-E_s)^2/E_s N_0)}\, dx \\ &= \frac{1}{\sqrt{\pi}} \int_{(R_0 - E_s/\sqrt{E_s N_0}}^{\infty} e^{-x^2}\, dx \\ &= \frac{1}{2} \operatorname{erfc}\left(\frac{R_0 - E_s}{\sqrt{E_s N_0}}\right) \end{aligned} \tag{92}$$

For the noncoherent detection, the in-phase and the quadrature components from Eq. (86) are

$$\begin{aligned} X_c &= \int_0^T r(t)\cos(2\pi f_0 t)\, dt = \int_0^T A\cos(2\pi f_0 t + \theta)\cos(2\pi f_0 t)\, dt \\ &\quad + \int_0^T n(t)\cos(2\pi f_0 t)\, dt = \frac{AT}{2}\cos\theta \\ &\quad + \int_0^T n(t)\cos(2\pi f_0 t)\, dt \\ X_s &= \frac{AT}{2}\sin\theta + \int_0^T n(t)\cos(2\pi f_0 t)\, dt \end{aligned} \tag{93}$$

For white Gaussian noise with two-sided spectral density $N_0/2$, we have the following quantities:

$$\begin{aligned} E[X_c] &= \frac{AT}{2}\cos\theta \\ E[X_s] &= \frac{AT}{2}\sin\theta \\ \operatorname{Var}[X_c] &= \operatorname{Var}[X_s] \\ &= E\left[\int_0^T \int_0^T n(s)n(t)\cos(2\pi f_0 t)\cos(2\pi f_0 s)\, dt\, ds\right] \\ &= \frac{N_0 T}{4} \end{aligned} \tag{94}$$

and therefore the joint probability density functions can be written as

$$\begin{aligned} p_1(X_c, X_s|\theta) &= \frac{1}{\pi N_0 T/2} \\ &\qquad \exp\left(-\frac{(X_c - AT\cos\theta/2)^2 + (X_s - AT\sin\theta/2)^2}{N_0 T/2}\right) \\ p_0(X_c, X_s) &= \frac{1}{\pi N_0 T/2}\exp\left(-\frac{X_c^2 + X_s^2}{N_0 T/2}\right) \end{aligned} \tag{95}$$

under the H_1 and H_0 hypotheses, respectively. The averaged joint probability density function of $p_1(X_c, X_s|\theta)$ is

$$\begin{aligned} p_{1,\text{av}}(X_c, X_s|\theta) &= \int_0^{2\pi} \frac{1}{2\pi} p_1(X_c, X_s|\theta)\, d\theta \\ &= \int_0^{2\pi} \frac{1}{2\pi} \frac{1}{\pi N_0 T/2} \\ &\exp\left(-\frac{X_c^2 + X_s^2 - AT(\cos\theta)X_c - AT(\sin\theta)X_s + A^2T^2/4}{N_0 T/2}\right) d\theta \\ &= \frac{1}{\pi N_0 T/2} \exp\left(-\frac{X_c^2 + X_s^2 + A^2T^2/4}{N_0 T/2}\right) \\ &I_0\left(\frac{2\sqrt{A^2T^2(X_c^2 + X_s^2)/4}}{N_0 T/2}\right) \end{aligned} \tag{96}$$

For an envelope ($V = \sqrt{X_c^2 + X_s^2}$ detection, let $X_c = V\cos\theta$, $X_s = V\sin\theta$, then $dX_c dX_s = V\, dV\, d\theta$. We have

$$\begin{aligned} p_{1,\text{av}}(V) &= \int_0^{2\pi} p_{1,\text{av}}(V, \theta)\, d\theta \\ &= \int_0^{2\pi} \frac{V}{\pi N_0 T/2} \exp\left(-\frac{V^2 + A^2T^2/4}{N_0 T/2}\right) I_0\left(\frac{2AV}{N_0}\right) d\theta \\ &= \frac{4V}{N_0 T} \exp\left(-\frac{V^2 + A^2T^2/4}{N_0 T/2}\right) I_0\left(\frac{2AV}{N_0}\right) \end{aligned} \tag{97}$$

which is a Rice distribution.

Under the H_0 hypothesis, we substitute $A = 0$ and use $I_0(0) = 1$ in Eq. (97) to obtain the following Rayleigh distribution:

$$p_0(V) = \frac{4V}{N_0 T} \exp\left(-\frac{V^2}{N_0 T/2}\right) \tag{98}$$

The threshold R_0 is therefore determined from the false-alarm probability P_{fa} using

$$P_{\text{fa}} = \int_{R_0}^{\infty} \frac{4V}{N_0 T} \exp\left(-\frac{V^2}{N_0 T/2}\right) dV = \exp\left(-\frac{R_0^2}{N_0 T/2}\right) \tag{99}$$

as

$$R_0 = \sqrt{-\frac{N_0 T}{2} \ln P_{\text{fa}}} \tag{100}$$

And the detection probability P_d is given by

$$P_d = \int_{R_0}^{\infty} \frac{4V}{N_0 T} \exp\left(-\frac{V^2 + A^2T^2/4}{N_0 T/2}\right) I_0\left(\frac{2AV}{N_0}\right) dV \quad (101)$$

This can be put into a more convenient dimensionless form with the changing of variable $x = \sqrt{N_0 T/4}$ from which

$$P_d = \int_{(-2\ln P_{fa})^{1/2}}^{\infty} x \exp\left(-\frac{x^2 + \alpha^2}{2}\right) I_0(\alpha x)\, dx \quad (102)$$

where

$$\alpha^2 = A^2 T/N_0 = 2E_s/N_0 \quad (103)$$

For a square-law ($Z = X^2{}_c + X^2{}_s$) detection, let $X_c = \sqrt{Z}\cos\theta, X_s = \sqrt{Z}\sin\theta$; then $dX_c dX_s = \frac{1}{2}\, dZ\, d\theta$. From Eq. (96) we have

$$\begin{aligned} p_{1,av}(Z) &= \int_0^{2\pi} \frac{1}{\pi N_0 T} \exp\left(-\frac{Z + A^2T^2/4}{N_0 T/2}\right) I_0\left(\frac{\sqrt{A^2T^2Z}}{N_0 T/2}\right) d\theta \\ &= \frac{2}{N_0 T} \exp\left(-\frac{Z + A^2T^2/4}{N_0 T/2}\right) I_0\left(\frac{\sqrt{A^2T^2Z}}{N_0 T/2}\right) \end{aligned} \quad (104)$$

which is a noncentral χ^2 distribution. Under H_0, we have the following central χ^2 distribution:

$$p_0(Z) = \frac{2}{N_0 T} \exp\left(-\frac{Z}{N_0 T/2}\right) \quad (105)$$

The threshold R_0 can be determined from the false-alarm probability P_{fa}, which is given by

$$P_{fa} = \int_{R_0}^{\infty} \frac{2}{N_0 T} \exp\left(-\frac{Z}{N_0 T/2}\right) dZ = \exp\left(-\frac{R_0}{N_0 T/2}\right) \quad (106)$$

to be

$$R_0 = -\frac{N_0 T}{2} \ln P_{fa} \quad (107)$$

The detection probability P_d is given by

$$P_d = \int_{R_0}^{\infty} \frac{2}{N_0 T} \exp\left(-\frac{Z + A^2T^2/4}{N_0 T/2}\right) I_0\left(\frac{\sqrt{A^2T^2Z}}{N_0 T/2}\right) dZ \quad (108)$$

Changing the variable $x = Z/N_0T/4$ in Eq. (108) yields a more convenient dimensionless form

$$P_d = \int_{-2\ln P_{fa}}^{\infty} \tfrac{1}{2} \exp\left(-\frac{x+\alpha^2}{2}\right) I_0(\alpha\sqrt{x})\, dx \qquad (109)$$

where α is given by Eq. (103). Changing the variable $y = \sqrt{x}$ in Eq. (109) leads to the interesting result that P_d is identical to that given by Eq. (102) for the envelope detection. Note that the difference between the envelope and the square-law detector concerns the presence or absence of the square-root operation. Supposing for a square-law detection that an observation value is greater than R_0 of Eq. (107); then the square root of this value must be greater than R_0 of Eq. (100) for the envelope detection. Therefore, the square-law detection and the envelope detection bear the same detection characteristics.

The P_d's in Eqs. (92), (102), and (109) show explicitly that the detection probabilities depend only on P_{fa} and the signal-to-noise ratio E_s/N_0. Note that, in addition to P_{fa}, the detection threshold R_0 depends on the received signal energy in the coherent case of Eq. (91), but only on the noise and the integration time in the noncoherent case of Eqs. (100) and (107), which is somewhat more convenient.

A comparison of coherent and noncoherent detections is presented in Fig. 14 in terms of the value of P_d that can be achieved for a given value of P_{fa} as a function of signal-to-noise ratio E_s/N_0. We note the following: (1) For small values of E_s/N_0 (say less than 3 dB) for any given value of P_{fa}, noncoherent detection requires from 2 dB to 3 dB more SNR than that required by coherent detection in order to achieve the same value of detection. (2) For large values of E_s/N_0 (say greater than 10 dB) the difference in SNR required by the two schemes is less than approximately 1 dB, and it is clear that with further increase E_s/N_0, the difference eventually becomes negligible.

Output Signal-to-Noise Analysis. To evaluate the detection performance, we can compare output SNRs of different schemes other than the detection probabilities we used in the last section. Recall that the SNR is the ratio between the signal power and the noise variance. The signal power is the square of the mean of the detection statistic under H_1. Thus only the mean and the variance are required to compute the SNR. In contrast, the detection probability requires full knowledge of the probability density function, which may not be available sometimes. Therefore the output SNR, which is easier to obtain, is also used to evaluate the detection performance. Of course the detection-probability-based performance evaluation, if it is available, is more accurate than the SNR-based evaluation. In this section, the output SNR will be used to compare the detection performance between the matched filter and the square-law detection.

The matched filter output Y for an input signal $A\cos(2\pi f_0 t)$ can be written as

$$Y = \int_0^T [A\cos(2\pi f_0 t) + n(t)]\cos(2\pi f_0 t)\, dt \qquad (110)$$

The band-pass noise $n(t)$ can be expressed in the form

$$n(t) = n_c(t)\cos(2\pi f_0 t) + n_s(t)\sin(2\pi f_0 t) \qquad (111)$$

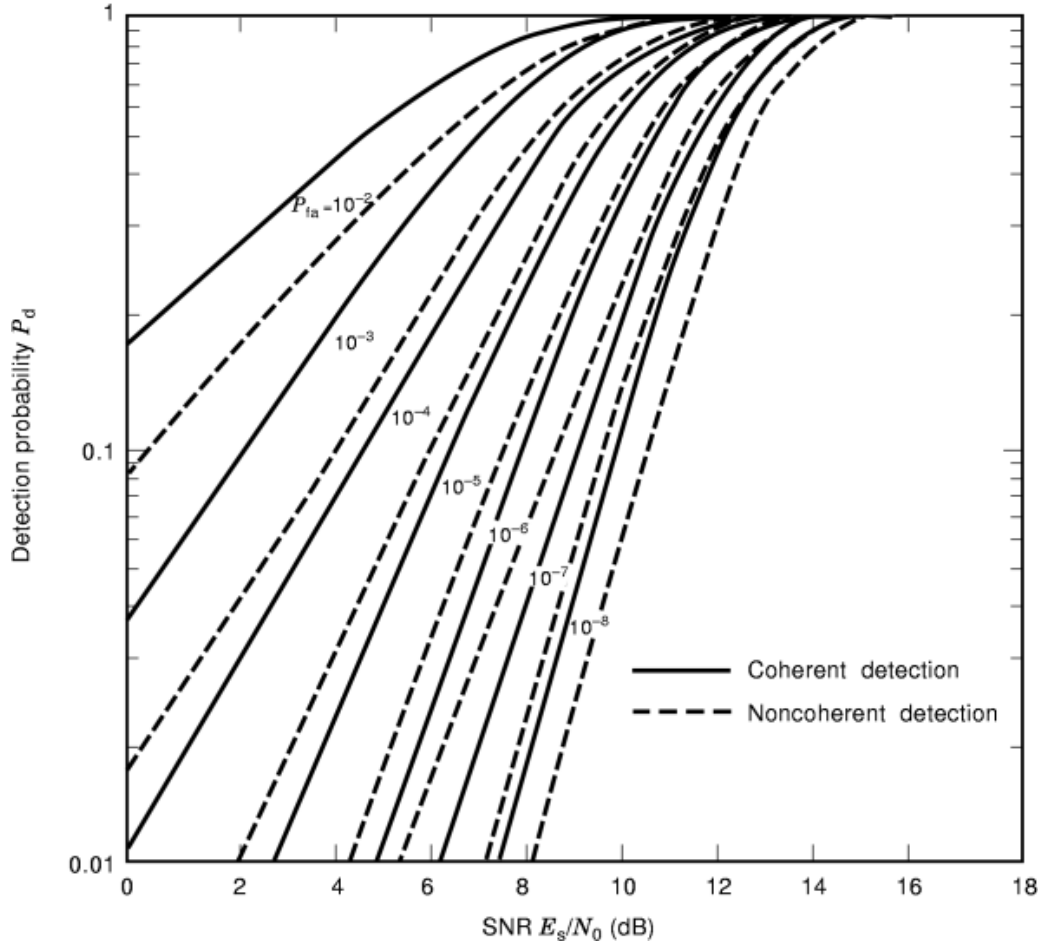

Fig. 14. Detection probability for coherent and noncoherent detection.

Hence

$$Y = \frac{AT}{2} + \int_0^T [n_c(t)\cos(2\pi f_0 t) + n_s(t)\sin(2\pi f_0 t)]\cos(2\pi f_0 t)\,dt$$
$$= \frac{AT}{2} + \frac{n_c(t)T}{2} \tag{112}$$

Equation (112) indicates that the quadrature noise $n_s(t)\sin(2\pi f_0 t)$ has been rejected by the low-pass filter from the output. The first term in Eq. (112) is the signal component with output signal power $A^2T^2/4$, while the second term represents the in-phase noise component with output noise power $E[n^2{}_c(t)]T^2/4$. Using Ref. 2

$$E[n_c^2(t)] = E[n_s^2(t)] = E[n^2(t)] = \sigma^2 \tag{113}$$

we obtain the output SNR

$$\mathrm{SNR}_{\mathrm{out}} = \frac{A^2}{\sigma^2} \tag{114}$$

The input signal power is $A^2/2$ and the input noise power is $E[n^2(t)] = \sigma^2$. The input SNR is therefore

$$\mathrm{SNR}_{\mathrm{in}} = \frac{A^2}{2\sigma^2} \tag{115}$$

and we have the following relationship between the input and output SNRs for coherent detection:

$$\mathrm{SNR}_{\mathrm{out}} = 2\mathrm{SNR}_{\mathrm{in}} \tag{116}$$

It is clear that coherent detection gives a 3 dB improvement in SNR. The reason for this improvement is that the multiplier and low-pass filter in Eq. (110) eliminate the quadrature noise component $n_s(t)\sin(2\pi f_0 t)$.

On the other hand, in the noncoherent case both the in-phase and the quadrature noise components come in to play. To analyze the square-law detection easily, we use the equivalent scheme of Fig. 12 with the square-law rectifier characteristic of $y = x^2$, as shown in Fig. 13(c), replacing the linear rectifier. The output Z of a square-law detection for the following received signal:

$$A\cos(2\pi f_0 t) + n_c(t)\cos(2\pi f_0 t) + n_s(t)\sin(2\pi f_0 t) \tag{117}$$

can be written as (4)

$$Z = \frac{T}{2}[A^2 + 2An_c(t) + n_c^2(t) + n_s^2(t)] \tag{118}$$

This output can be regarded as composed of three terms. The first term, $A^2T/2$, is the desired output signal component with output signal power $(A^2T/2)^2$. The second term, $ATn_c(t)$, represents the carrier-noise component with the associated output noise power $A^2T^2\sigma^2$. The third term, $\frac{1}{2}[n^2{}_c(t) + n^2{}_s(t)]$, is the self-noise component. The associated noise power is

$$\begin{aligned} &\frac{T^2}{4}E\{[n_c^2(t) + n_s^2(t)]^2\} - \frac{T^2}{4}\{E[n_c^2(t) + n_s^2(t)]\}^2 \\ &= \frac{T^2}{2}\{E[n_c^4(t)] + \{E[n_c^2(t)]\}^2\} - T^2\{E[n_c^2(t)\}^2 \\ &= T^2\sigma^4 \end{aligned} \tag{119}$$

where $E[n^4(t)] = 3\{E[n^2(t)]\}^2 = 3\sigma^4$ has been used in the last step. With these results, we can write the output SNR as

$$\mathrm{SNR}_{\mathrm{out}} = \frac{A^4/(4\sigma^4)}{A^2/\sigma^2 + 1} = \frac{\mathrm{SNR}_{\mathrm{in}}^2}{2\mathrm{SNR}_{\mathrm{in}} + 1} \tag{120}$$

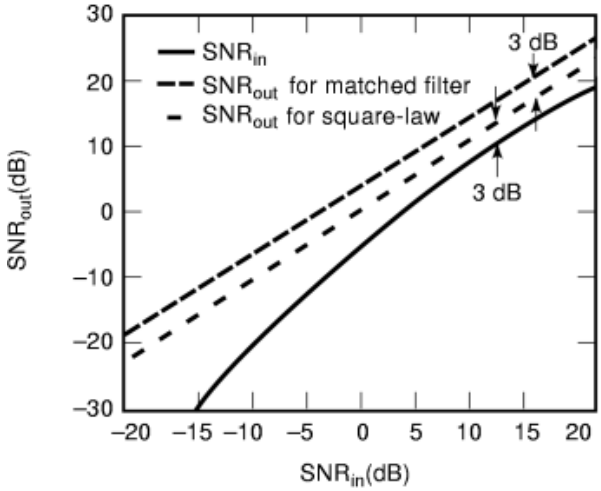

Fig. 15. Output signal-to-noise ratios for the matched filter and the square-law detection.

If the input SNR is much larger than 1, the output SNR is approximately equal to $\frac{1}{2}\text{SNR}_{\text{in}}$, with the square-law detection thus causing a 3 dB reduction in signal-to-noise ratio. For input signal-to-noise ratios that are much less than 1, 2SNR_{in} is negligible compared with 1, and Eq. (120) shows that SNR_{out} is now equal to SNR^2_{in}. In this case, the square-law detection causes a very serious degradation of the signal-to-noise ratio.

The relationship between SNR_{out} and SNR_{in} for the matched filter and the square-law detection is shown in Fig. 15. It is clear from both Fig. 14 and Fig. 15 that the noncoherent detection is inferior to the coherent detection for low input signal-to-noise ratios and approximates the coherent detection for high input signal-to-noise ratios in the detection probability and the output signal-to-noise ratio.

Detection of the Linear Frequency-Modulated Signal

In the previous sections, we have considered the detection of the narrow-band signal such as the single-frequency sinusoidal pulses given by Eq. (79). The product of time duration T and bandwidth B is essentially 1. There is an inherent conflict between long-range detection and high-range-resolution capability for such signals. Because the received signal energy E_s attenuates rapidly as the range increases, the long range requires large transmitted signal amplitudes in order to have a sufficiently large value of E_s/N_0 for reliable detection and range estimation. But all radar systems have a limitation on the peak transmitted signal power, which imposes an upper limit on the transmitted signal amplitude. Of course the required value of E_s can also be obtained by maintaining the transmitted signal amplitude at some maximum value A and increasing the signal duration T. In this case the signal bandwidth B, which is approximately $1/T$, is small. But since the signal bandwidth B is inversely proportional to the range resolution (5), then achieving the required E_s by increasing T reduces B, thereby degrading range-resolution capability.

On the other hand, if B can be increased essentially independently of T, there is no such conflict. This is why modern radar systems employ large time–bandwidth product (BT) signals. In the radar system, the earliest and most widely used large BT signal is the linear frequency-modulated (*LFM*) signal (1,3). In addition to providing a solution to the long-range–high-resolution problem, the LFM signal is also a form of Doppler-invariant waveform (3).

We note that in military communication systems, a large time–bandwidth product signal is referred to as a spread-spectrum signal (2). It provides resistance to jamming and has a low interception probability because the signal is transmitted at low power. Among various spread-spectrum signals, the direct sequence spread spectrum (*DSSS*) signal, where the transmitted signal is modulated by a pseudorandom sequence, is used in code devision multiple access (*CDMA*) communications (6). The frequency-hopped spread spectrum (*FHSS*) is another widely used spread spectrum signal in modern communication systems (2,7).

Wigner-Ville Distribution and Ambiguity Function of an LFM Signal. For an LFM signal the analytic form is

$$s(t) = \begin{cases} \exp\left[j\left(2\pi f_0 t + \dfrac{m}{2}t^2\right)\right], & 0 \le t \le T \\ 0, & \text{otherwise} \end{cases} \tag{121}$$

The instantaneous frequency in Eq. (121) is

$$f_i(t) = f_0 + mt \tag{122}$$

which has an initial frequency f_0 and increases at a frequency rate m. Since an LFM signal is a nonstationary signal, the best way to describe it is through such distribution functions as the Wigner-Ville distribution (*WVD*) and the ambiguity function (*AF*). The WVD of a signal $s(t)$ is defined as

$$\text{WVD}(t, f) = \int_{-\infty}^{\infty} s(t + \tau/2)s^*(t - \tau/2)e^{-j2\pi f\tau}\, d\tau \tag{123}$$

WVD is the Fourier transform (with respect to the delay τ) of the signal's correlation function. It relates the time and the instantaneous frequency of a signal. Substituting the LFM signal of Eq. (121) into this definition yields [15]

$$\text{WVD}(t, f) = \begin{cases} 2(T - 2|t - T/2|)\text{sinc}[(T - 2|t - T/2|)[f - f_i(t)]], \\ \qquad\qquad 0 \le t \le T \\ 0, \qquad\qquad \text{otherwise} \end{cases} \tag{124}$$

where $f_i(t)$ is given in Eq. (122) and the sine function is defined as

$$\text{sinc}(t) = \begin{cases} \sin(\pi t)/(\pi t) & t \ne 0 \\ 1 & t = 0 \end{cases}$$

Figure 16 shows the WVD for an LFM signal with $f_0 = 20$, $m = 12$, and $T = 2$. It is seen from the WVD that the instantaneous frequency linearly increases with the time in accordance with Eq. (122), whereas this relationship is not observable from the spectrum of the signal, which is also shown at the top of Fig. 16.

The ambiguity function (*AF*) is defined as

$$\text{AF}(\tau, \xi) = \int_{-\infty}^{\infty} s(t + \tau/2)s^*(t - \tau/2)e^{-j2\pi\xi t}\, dt \tag{125}$$

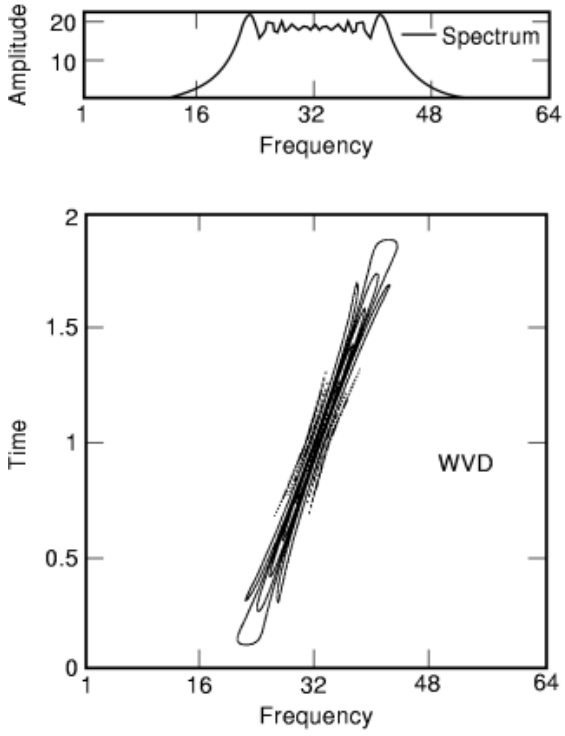

Fig. 16. Spectrum (top) and WVD (bottom) of an LFM signal.

where ξ and τ denote the frequency shift and the delay, respectively. AF is the Fourier transform (with respect to the time t) of the signal's correlation function, and it relates the delay and the Doppler frequency (or frequency shift). Note that the AF and the WVD form a two-dimensional (2-D) Fourier pair, that is,

$$\underset{\tau\to f}{\mathscr{F}}\,\underset{\xi\to t}{\mathscr{F}^{-1}}[\mathrm{AF}(\tau,\xi)] = \int_{-\infty}^{\infty}\int_{-\infty}^{\infty}\mathrm{AF}(\tau,\xi)e^{j2\pi\xi t}e^{-j2\pi f\tau}\,d\xi\,d\tau = \mathrm{WVD}(t,f) \tag{126}$$

where $\mathscr{F}$ and $\mathscr{F}^{-1}$ denote the Fourier and its inverse operators, respectively. Applying Parseval's theorem $\int u(t)v*(t)\,dt = \int U(f)V*(f)\,df$ to Eq. (125), we obtain

$$\mathrm{AF}(\tau,\xi) = \int_{-\infty}^{\infty} S^*(f)S(f+\xi)e^{j2\pi f\tau}\,df \tag{127}$$

The AF can therefore be regarded as the matched-filter output with a different delay τ and frequency shift ξ.

The AF has proven to be an important tool in analyzing and constructing radar signals by relating range and velocity resolutions. By constructing signals having a particular ambiguity function, desired performance

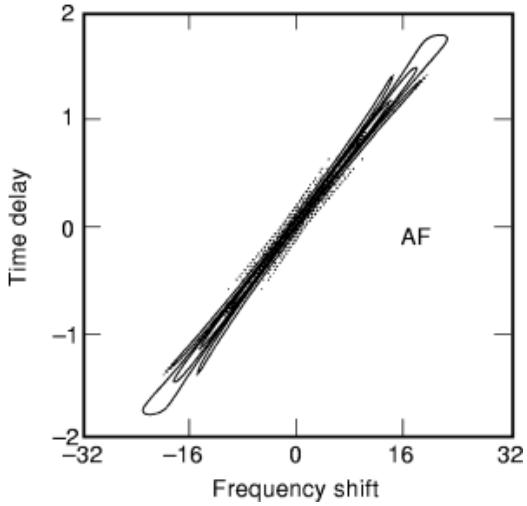

Fig. 17. Ambiguity function of the LFM signal. The AF is symmetric about the origin, and its greatest value appears above the origin.

characteristics are achieved. For example, the magnitude AF of the LFM signal in Eq. (121) is

$$|\mathbf{AF}(\tau,\xi)| = \begin{cases} (T-|\tau|)\mathrm{sinc}[(T-|\tau|)(\xi-m\tau)], & |\tau| \le T \\ 0, & \text{otherwise} \end{cases} \tag{128}$$

which is shown in Fig. 17 for the same LFM signal in Fig. 16. The AF is symmetric about the origin $\tau = \xi = 0$, and the greatest value appears above the origin. The time delay τ is related to the range, and the frequency shift ξ is related to the Doppler shift. Thus AF describes the range-Doppler ambiguity of the transmitted signal. An ideal radar signal is the one whose AF is a thumbtack function because it leaves the least ambiguity in resolving the range and Doppler shift.

Detection of Multiple LFM Signals. The matched-filter detection is the optimal detection if all of the signal information (phase, initial frequency, and frequency rate) is available. However, these parameters are difficult to specify because accurate values of the range, the velocity, and the acceleration of a target are not available. Noncoherent detection is thus preferred. Next, we are going to consider the noncoherent detection of *multiple* LFM signals in a noise background.

For multiple LFM signal detection, it is often the case that the frequency rate is the only parameter of interest in practice (8). In other words, the frequency rates distinguish different LFM signals. Such a scenario occurs in the radar detection of a small, fast-moving missile launched from a relatively slow-moving aircraft. Multiple LFM signals can be detected by locating maxima in the frequency rate in many applications.

AF of Multiple LFM Signals. The input signal to be analyzed is modeled by a linear sum of two (may be extended to more than two) LFM signals with frequency rates m_0 and m_1 as given by

$$r(t) = \sum_{i=0}^{1} \exp\left[j\left(\omega_i t + \frac{1}{2}m_i t^2\right)\right] \tag{129}$$

Here ω_i represent the carrier (or the initial) frequency, which is proportional to the velocity of the target, and the frequency rate m_i is proportional to the acceleration. The AF defined by

$$\mathrm{AF}_r(\tau,\omega)=\int_{-\infty}^{\infty} r(t+\tau/2)r^*(t-\tau/2)e^{-j\omega t}\,dt \tag{130}$$

is computed for the signal $r(t)$ of Eq. (129) to yield

$$\begin{aligned}\mathrm{AF}_r(\tau,\omega)=&\delta(\omega-m_0\tau)e^{j\omega_0\tau}+\delta(\omega-m_1\tau)e^{j\omega_1\tau}\\&+\exp\left[j\left(\frac{\omega_0+\omega_1}{2}\tau+\frac{m_0-m_1}{8}\tau^2\right)\right]Q_1\\&+\exp\left[j\left(\frac{\omega_0+\omega_1}{2}\tau+\frac{m_1-m_0}{8}\tau^2\right)\right]Q_2\end{aligned} \tag{131}$$

where

$$\begin{aligned}Q_1=&\exp\left(-j\frac{[-2\omega+(m_0+m_1)r+2\omega_0-2\omega_1]^2}{8(m_0-m_1)}\right)\int_{-\infty}^{\infty}\\&\exp\left[j\frac{m_0-m_1}{2}\left(t+\frac{-2\omega+(m_0+m_1)r+2\omega_0-2\omega_1}{2(m_0-m_1)}\right)^2\right]dt\\Q_2=&\exp\left(-j\frac{[-2\omega+(m_0+m_1)r+2\omega_1-2\omega_0]^2}{8(m_1-m_0)}\right)\int_{-\infty}^{\infty}\\&\exp\left[j\frac{m_1-m_0}{2}\left(t+\frac{-2\omega+(m_0+m_1)r+2\omega_1-2\omega_0}{2(m_1-m_0)}\right)^2\right]dt\end{aligned}$$

The last two terms of Eq. (131) are interference terms generated by the two LFM components in the signal $r(t)$, due to the nonlinearity of the AF. Using the following identity

$$\int_{-\infty}^{\infty} e^{-jmt^2}\,dt=\sqrt{\frac{\pi}{m}}\exp\left(-j\frac{\pi}{4}\right),\quad m>0 \tag{132}$$

Q_1 and Q_2 are combined to give

$$\begin{aligned}\mathrm{AF}_r(\tau,\omega)=&\delta(\omega-m_0\tau)e^{j\omega_0\tau}+\delta(\omega-m_1\tau)e^{j\omega_1\tau}+2\sqrt{\frac{2\pi}{m_0-m_1}}\\&\times\exp\left[j\left(\frac{\omega(\omega_0-\omega_1)+\omega_1 m_0\tau-\omega_0 m_1\tau}{m_0-m_1}\right)\right]\\&\mathrm{Re}\left\{\exp\left[j\left(\frac{m_0 m_1\tau^2+\omega^2+(\omega_0-\omega_1)^2-\omega(m_0+m1)\tau}{2(m_0-m_1)}-\frac{\pi}{4}\right)\right]\right\}\end{aligned} \tag{133}$$

Figure 18(a) shows the AF [Eq. (133)] of a signal composed of two LFM signals which may represent two targets with different velocities and accelerations. Although there is cross-term interference, we can identify

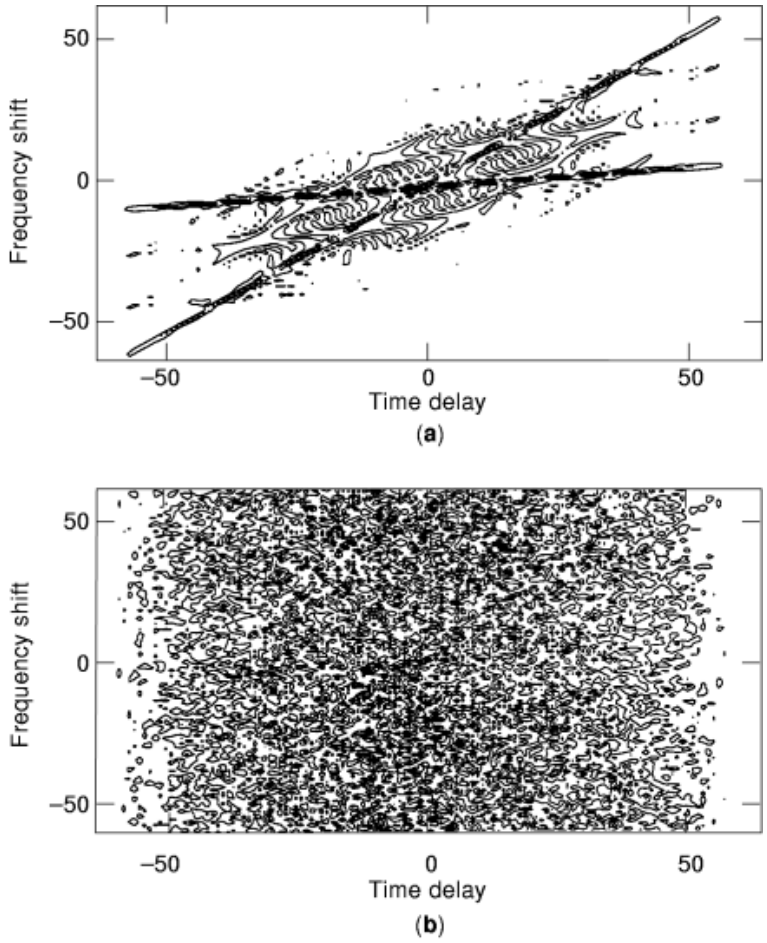

Fig. 18. The ambiguity functions of a bicomponent LFM signal (a) without noise, and (b) with the additive white Gaussian noise (SNR = −6 dB).

the two straight lines representing the bicomponent signal in Fig. 18(a). However, the two LFM signals are not obvious if they are corrupted by noise. Figure 18(b) is identical to Fig. 18(a) except that the two signals are corrupted by Gaussian white noise with SNR = −6 dB.

Detecting Multiple LFM Signals Using Radon-Ambiguity Transform. Recall that the Radon transform (9), commonly used for the reconstruction of images in computer tomography, is defined by

$$R_{s,\phi}\{f(x,y)\} = \int_{-\infty}^{\infty}\int_{-\infty}^{\infty} f(x,y)\delta(x\sin\phi + y\cos\phi - s)\,dxdy \tag{134}$$

for $-\infty < s < \infty$ and $-\pi/2 < \phi < \pi/2$, where the δ function specifies the direction of integration. The parameter s represents the shifted location of the origin. Equation (134) actually represents the sum of the values of $f(x, y)$ along the line that makes an angle ϕ with the x axis and is located at a distance s from the origin. The Radon–Wigner transform 9, 10 is a special case when $f(x, y)$ in Eq. (134) takes the WVD of a multicomponent LFM

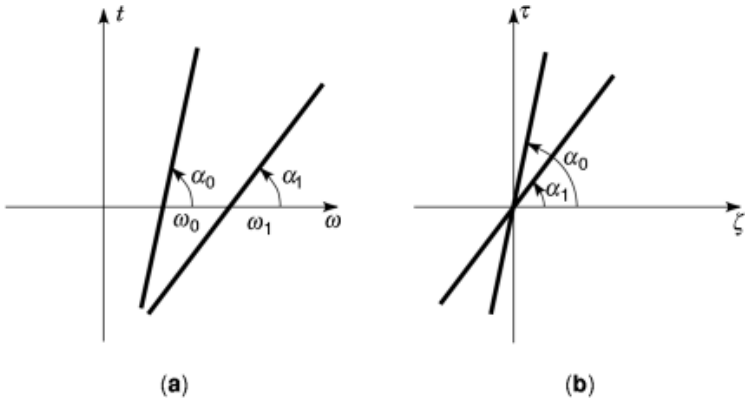

Fig. 19. (a) The WVD of a bicomponent signal. (b) the AF of the bicomponent signal.

signal. The WVD of a bicomponent signal is graphically drawn in Fig. 19(a). The Radon–Wigner transform of Fig. 19(a) should produce two maxima in the resulting α-ω plane. Figure 19(b) is the AF of the same signal in Fig. 19(a). The AF is the 2-D Fourier transform of the WVD; thus they share the same angles of α_0 and α_1 as shown in the WVD. However, the initial frequencies shown in Fig. 19(a) have disappeared in Fig. 19(b), since they have been mapped into the phase of the AF. This also explains why the AFs of the two chirps pass through the origin in the τ-ξ plane. Thus, by applying the Radon transform to the *phase-free* ambiguity function, detection of multicomponent signals can be reduced from the 2-D search problem in the Radon–Wigner transform to a 1-D search problem. The advantage of the ambiguity function over the WVD has been shown in the kernel design for the time-frequency analysis (11). This work can be extended to the detection of multicomponent signals (12).

Since all directions of interest pass through the origin of the ambiguity plane, the Radon transform with parameter s set to 0 is applied to the phase-free ambiguity function of Eq. (133). We essentially compute the line integral along a straight line with its direction specified by the δ function $\delta(\xi - m\tau)$ in the ambiguity plane. Therefore the detection statistic can be formed by the so-called Radon-ambiguity transform (12) as

$$\begin{aligned} \eta(m) &= \int_{-\infty}^{\infty}\int_{-\infty}^{\infty} |\mathbf{AF}_r(\tau,\xi)|\delta(\xi - m\tau)\,d\tau\,d\xi \\ &= \int_{-\infty}^{\infty} |\mathbf{AF}_r(\tau, m\tau)|\,d\tau \end{aligned} \tag{135}$$

Since the infinite integrals in Eq. (135) usually diverge, it is necessary to first remove the constant term from the integrand. Specifically, for $m \neq m_i$ $(i = 0, 1)$ and assuming $m_0 - m_1 > 0$, we have from Eq. (133)

$$\begin{aligned} &|\mathbf{AF}_r(\tau, m\tau)| \\ &\quad = \left| 2\sqrt{\frac{2\pi}{m_0 - m_1}}\,\mathbf{cos}(a_m\tau^2 + b) \right| \\ &\quad = 4\sqrt{\frac{2}{\pi(m_0 - m_1)}}\left(1 + \sum_{n=1}^{\infty}\frac{2(-1)^{n-1}}{(2n)^2 - 1}\,\mathbf{cos}(2na_m\tau^2 + 2nb)\right) \end{aligned} \tag{136}$$

with

$$a_m = \frac{m_0 m_1 + m^2 - m(m_0 + m_1)}{2(m_0 - m_1)},\ b = \frac{(\omega_0 - \omega_1)^2}{2(m_0 - m_1)} - \frac{\pi}{4} \quad (137)$$

Removing the constant from Eq. (136) and substituting it into Eq. (135) yield

$$\eta(m) = 4\sqrt{\frac{2}{a_m(m_0 - m_1)}} \sum_{n=1}^{\infty} \frac{2(-1)^{n-1}}{(2n)^2 - 1} \sqrt{\frac{1}{n}} \sin\left(2nb + \frac{\pi}{4}\right) \quad (138)$$

For $m \neq m_0$ or m_1 (i.e., $a_m \neq 0$), it is clear that $\eta(m)$ is finite. By Eqs. (137) and (138), we have $\eta(m) \to \infty$ as $m \to m_0$ or $m \to m_1$. Therefore, by calculating $\eta(m)$ and comparing it to a preset threshold, the multicomponent signals can be detected.

Finite-Length Signal. Now we consider a bicomponent finite-length signal as given by

$$r(t) = \begin{cases} \dfrac{1}{\sqrt{T}} \exp\left[j\left(\omega_0 t + \dfrac{1}{2} m_0 t^2\right)\right] + \dfrac{1}{\sqrt{T}} \exp\left[j\left(\omega_1 t + \dfrac{1}{2} m_1 t^2\right)\right] & \text{for } |t| \leq \dfrac{T}{2} \\ 0 & \text{for } |t| > \dfrac{T}{2} \end{cases} \quad (139)$$

with the assumption that $\omega_0 = \omega_1$ and $m_0 > m_1$ for simplicity purposes. The modulus of the ambiguity function of $r(t)$ for $\omega = m\tau$ can be calculated by making use of the following integral,

$$\int e^{j(px^2 + 2qx)}\, dx = \sqrt{\frac{\pi}{2p}} e^{-jq^2/p} \left[C\left(\frac{px + q}{\sqrt{p}}\right) + jS\left(\frac{px + q}{\sqrt{p}}\right)\right] \quad (140)$$

to yield

$$|\mathrm{AF}_r(\tau, m\tau)| = \begin{cases} \left| \dfrac{2\sin\left((T - |\tau|)\dfrac{\tau}{2}(m - m_0)\right)}{T\tau(m - m_0)} + \dfrac{2\sin\left((T - |\tau|)\dfrac{\tau}{2}(m - m_1)\right)}{T\tau(m - m_1)} \right. \\ \quad + \dfrac{2}{T}\sqrt{\dfrac{\pi}{m_0 - m_1}} \times \{[C(X_0) + C(X_1)]\cos(a_m \tau^2) \\ \left. \quad + [S(X_0) + S(X_1)]\sin(a_m \tau^2)\} \right| & \text{for } |\tau| \leq T \\ 0 & \text{for } |\tau| > T \end{cases} \quad (141)$$

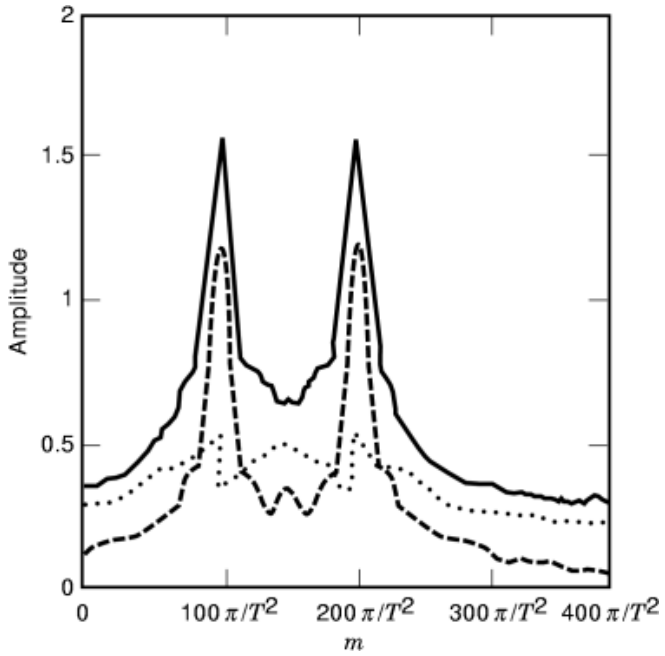

Fig. 20. The $\eta(m)$ of two equal-amplitude LFM signals with $T = 40$, $m_0 = 200\pi/T^2$, $m_1 = 100\pi/T^2$. Solid line: $\eta(m)$. Dashed line: auto terms only. Dotted line: cross-terms only. The two peaks indicate the existence of the equal-amplitude ∠FM signals.

where

$$C(x) = \int_0^x \cos\left(\frac{\pi t^2}{2}\right) dt, \qquad S(x) = \int_0^x \sin\left(\frac{\pi t^2}{2}\right) dt$$

are the Fresnel integrals, and

$$X_0 = \sqrt{\frac{m_0 - m_1}{8}}\left(T + \frac{2(-m + m_1)}{m_0 - m_1}\tau\right)$$
$$X_1 = \sqrt{\frac{m_0 - m_1}{8}}\left(T + \frac{2(m - m_0)}{m_0 - m_1}\tau\right)$$

while a_m in Eq. (141) is defined by Eq. (137). For $|\tau| \le T$, the first two terms in Eq. (141) represent the auto terms of the signal, while the rest express the cross-terms. Figure 20 shows the integral of Eq. (141) over τ, that is, $\eta(m)$, for two LFM signals with equal amplitudes. Also shown in Fig. 20 are the integrals of the auto terms and cross-terms of Eq. (141).

Output Signal-to-Noise Ratio Analysis. The output SNR of the statistics η in Eq. (135) can be analyzed by making use of the following quantities (12):

$$\begin{aligned} E(\eta|H_0) &= N_0 \\ E(\eta|H_1) &= A + N_0 \\ \mathrm{Var}(\eta|H_0) &= N_0^2 \\ \mathrm{Var}(\eta|H_1) &= 2AN_0 + N_0^2 \end{aligned}$$

to find

$$\mathrm{SNR}_{\mathrm{out}} = \frac{A^2}{2AN_0 + N_0^2} = \frac{\mathrm{SNR}_{\mathrm{in}}^2}{2\mathrm{SNR}_{\mathrm{in}} + 1} \qquad (142)$$

It is seen from Eq. (142) that there is a 3 dB loss in SNR between the input and the output when the input SNR is high, and the output SNR degrades severely when the input SNR is low, illustrating a typical nonlinear detection characteristic.

Conclusion

We have presented the techniques of radar signal detection, as well as the related performance analyses. The following conclusions can be drawn.

- Among various detection criteria, the Neyman–Pearson criterion is particularly well suited to radar detection, owing to its concepts of a priori fixed P_{fa} and maximized P_{d}.
- The coherent detection, in the form of a matched filter or a cross-correlation, is the optimal detection for an exactly known signal (i.e., phase, amplitude, and Doppler frequency are known) in a background of white noise.
- In a typical radar application, the range between the target and the radar represents a very large number of transmitted signal wavelengths. This makes specifying the phase of the return signal extremely difficult, and a noncoherent detection has to be used.
- The noncoherent detection is inferior to the coherent detection for low input signal-to-noise ratios and approximates the coherent detection for high input signal-to-noise ratios.
- There is an inherent conflict between long-range detection and high-range-resolution capability for the unity time-bandwidth signal. Large time-bandwidth signals such as an LFM signal do not have such a conflict.
- Large time-bandwidth signals can be described by the ambiguity function or the Wigner–Ville distribution. The Radon-ambiguity transform can be used to detect multiple LFM signals.

BIBLIOGRAPHY

1. C. E. Cook, M. Bernfeld, *Radar Signals: An Introduction to Theory and Application*, New York: Academic Press, 1967.
2. J. G. Proakis, M. Salehi, *Communication Systems Engineering*, Englewood Cliffs, NJ: Prentice-Hall, 1994.
3. J. Minkoff, *Signals, Noise, and Active Sensors*, New York: Wiley, 1992.
4. J. Brown, E. V. D. Glazier, *Signal Analysis*, New York: Reinhold, 1964.

5. D. L. Mensa, *High Resolution Radar Cross-Section Imaging*, Norwood, MA: Artech House, 1991.
6. A. J. Viterbi, *Principles of Spread Spectrum Communication*, Reading, MA: Addison-Wesley, 1995.
7. J. G. Proakis, *Digital Communications*, New York: McGraw-Hill, 1995.
8. P. M. Djuric, S. Kay, Parameter estimation of chirp signals, *IEEE Trans. Acoust. Speech Signal Process.*, **ASSP-38**: 2118–2126, 1990.
9. J. C. Wood, D. T. Barry, Tomographic time-frequency analysis and its application toward time varying filtering and adaptive kernel design for multicomponent linear-FM signals, *IEEE Trans. Signal Process.*, **42**: 2094–2104, 1994.
10. J. C. Wood, D. T. Barry, Radon transformation of time-frequency distributions for analysis of multicomponent signals, *IEEE Trans. Signal Process.*, **42**: 3166–3177, 1994.
11. B. Ristic, B. Boashash, Kernel design for time-frequency signal analysis using the radon transform, *IEEE Trans. Signal Process.*, **41**: 1996–2008, 1993.
12. M. Wang, A. K. Chan, C. K. Chui, Linear frequency modulated signal detection using radon-ambiguity transform, *IEEE Trans. Signal Process.*, **46**: 571–586, 1998.

READING LIST

M. Barkat, *Signal Detection and Estimation*, Norwood, MA: Artech House, 1991.
B. Bouachache, Time-frequency signal analysis, in S. Haykin (ed.), *Advances in Spectral Estimation and Array Processing*, Englewood Cliffs, NJ: Prentice-Hall, 1991, Vol. **1**, Chap. 9, pp. 418–517.
J. V. DiFranco, W. L. Rubin, *Radar Detection*, Englewood Cliffs, NJ: Prentice-Hall, 1968.
J. L. Eaves, E. K. Reedy (eds.), *Principles of Modern Radar*, New York: Van Nostrand-Reinhold, 1987.
G. Galati (ed.), *Advanced Radar Techniques and Systems*, Stevenage, UK: Peregrinus, 1993.
H. V. Poor, *An Introduction to signal Detection and Estimation*, New York: Springer, 1988.
D. C. Schleher, *MTI and Pulsed Doppler Radar*, Norwood, MA: Artech House, 1991.
H. Urkowitz, *Signal Theory and Random Processes*, Norwood, MA: Artech House, 1983.

MINSHENG WANG
Texas Instruments Incorporated
ANDREW K. CHAN
Texas A & M University